Vegetation and climate changes during the Early–Late Pliocene Transition (~3.6 Ma) in the Burdur Basin (Southwestern Anatolia): A comparison with the Mediterranean

Mary Robles[1], Valérie Andrieu[1], Pierre Rochette[1], Séverine Fauquette[2], Odile Peyron[2], François Demory[1], Oktay Parlak[3], Eliane Charrat[4], Belinda Gambin[5], Mehmet Cihat Alçiçek[6]

[1] Aix-Marseille Univ., CNRS, IRD, INRAE, UM 34 CEREGE, Aix-en-Provence, France
[2] Univ. Montpellier, CNRS, IRD, UMR 5554 ISEM, Montpellier, France
[3] Mineral Research and Exploration General Directorate, Ankara, Türkiye
[4] Aix-Marseille Univ., CNRS, IRD, INRAE, IMBE, Aix-en-Provence, France
[5] University of Malta, Institute of Earth Systems, Msida, Malta
[6] Pamukkale University, Department of Geology, Denizli, Türkiye

Correspondence to: Mary Robles (mary.robles@umontpellier.fr)

Abstract

The Early-Late Pliocene transition (~3.6 Ma) is a key period for understanding future climate change linked to increases in greenhouse gases. Around the Western Mediterranean Basin, the Early-Late Pliocene transition was marked by the establishment of a Mediterranean climate with summer droughts, cool/wet winters and latitudinal gradients. However, environmental changes in the eastern part of the Mediterranean area during the Early-Late Pliocene transition have rarely been documented. Here, we propose to reconstruct the environmental and climate changes during the Early-Late Pliocene transition from the Burdur Basin sequence, located in Southwestern Türkiye. This study aims to (1) characterize vegetation patterns, lake dynamics, and water level fluctuations using pollen and Non-Pollen Palynomorph (NPP) proxies, and (2) examine the morphological features of large Poaceae pollen grains (*Cerealia*-type). We also aim to quantitatively reconstruct climate changes through a multi-method approach, including the Modern Analogue Technique, Weighted Averaging Partial Least Squares regression, Random Forest, and Boosted Regression Trees and the Climatic Amplitude Method.

The results indicate that, during the Early-Late Pliocene transition at Burdur, the vegetation was dominated by steppes with Poaceae*, Artemisia*, and Amaranthaceae. Subsequently, arboreal taxa decreased and an alternation between steppe grasslands with deciduous *Quercus* and steppes dominated by Amaranthaceae became evident. The lacustrine ecosystem was characterized by semi-aquatic vegetation and freshwater algae, exhibiting alternating oligotrophic and eutrophic conditions. Large Poaceae pollen grains (*Cerealia*-type) are recorded in the Burdur Basin sequence, but their percentages are lower than those at Acıgöl to the west, a nearby record dated to the Pleistocene. The morphological characteristics of these large Poaceae pollen grains from Burdur are similar to those of domesticated cereals from recent periods, preventing a clear distinction between wild and domesticated Poaceae pollen. Pollen-inferred climate reconstructions show similar trends across the five methods, with reconstructed values during the Early-Late transition being close to present-day values at Burdur region. Following a climatic optimum in precipitation and temperature during the Early Pliocene, our results indicate an alternation between cool/wet conditions and warmer/drier conditions during the Late Pliocene in Southwestern Anatolia. Around the Mediterranean Basin, records show that the Early Pliocene had warmer conditions compared to modern

values and wetter conditions, with a north (wetter)-south (drier) gradient in terms of precipitation. The Late Pliocene is characterized by colder and more humid conditions in the Western Mediterranean, while the Eastern Mediterranean (Southwestern Türkiye) and Central Asia experienced more arid conditions. A weak Atlantic Meridional Overturning Circulation (AMOC) is identified in Europe during the Late Pliocene, leading to cooler and wetter conditions primarily in the Northwestern Mediterranean. While model simulations of PlioMIP2 show warmer conditions and a latitudinally contrasted precipitation pattern, with wetter conditions in Northern Europe and drier conditions in the south during the mid-Pliocene Warm Period (3.264–3.025 Ma).

Keywords

East Mediterranean; Pliocene; Paleoenvironment; Paleoclimate; Vegetation dynamics; Steppe ecosystems; Palynology; Transfer functions; Poaceae; Proto-cereals.

1. Introduction

The Pliocene Epoch (5.33-2.58 Ma), which was warmer than the pre-industrial period, is particularly important for understanding future climate change due to its similarities with present-day conditions, including comparable climatic characteristics (Haywood et al., 2016) and atmospheric CO_2 concentrations (Masson-Delmotte et al., 2013). During the mid-Pliocene Warm Period (mPWP; 3.264–3.025 Ma), atmospheric CO_2 concentration are estimated to have reached 350-450 p.p.m.v. (Raymo et al., 1996; Pagani et al., 2010), the Northern and West Antarctic ice sheets were smaller (Brierley et al., 2009; Fedorov et al., 2013), and sea levels were significantly higher than today, reaching about 20 m above the present-day value (Miller et al., 2012; Grant et al., 2019). Considering future climate change, Earth System Model (ESM) projections, based on CO_2 concentrations, ranging from about 400 p.p.m.v. to above 1100 p.p.m.v., indicate mass loss from the Greenland and Antarctic ice sheets, a projected sea-level rise of approximately 0.26 m to 0.92 m above present-day levels, and an increase in global air temperatures ranging from 1.4°C to 4.4°C depending on the scenario (IPCC, 2021, 2023). During the mid-Pliocene Warm Period, General Circulation Model (GCM) simulations suggest that the average temperature was approximately 3°C higher than in the pre-industrial period and that the temperature increase was particularly pronounced in the Northern Hemisphere high latitudes, where mean annual temperatures reached as high as 18°C (Haywood et al., 2013, 2020; Salzmann et al., 2013; Panitz et al., 2016). The Pliocene is divided into two periods (Haywood et al., 2016): (1) the Early Pliocene (Zanclean Age; 5.3-3.6 Ma), a warm period primarily characterized by 19-23 ka oscillations linked to precession orbital cycles, and (2) the Late Pliocene (Piacenzian Stage; 3.6-2.58 Ma) a generally colder period dominated by 19-23 ka and 41 ka oscillations linked to precession and obliquity orbital cycles (Haywood et al., 2009). The decrease in temperatures led to the initiation of the Northern Hemisphere glaciation from 3.6 to 2.4 Ma (Mudelsee and Raymo, 2005). Moreover, two major cooling events are evidenced at the Early-Late Pliocene transition (~3.6 Ma), the Marine isotope stages (MIS) MG12 at ~3.58 Ma and the MIS M2 at ~3.3 Ma (Lisiecki and Raymo, 2005; De Schepper et al., 2014).

The Early Pliocene was characterized by Mediterranean climate conditions (summer droughts and cool-wet winters) in the Western Mediterranean Basin, while Northern and Central Europe experienced more pronounced continental conditions (Suc, 1984; Suc et al., 2018). This climate pattern became established after the MIS M2 glacial event at ~3.3 Ma (Lisiecki and Raymo, 2005; Bertini, 2010; Jiménez-Moreno et al., 2010; De

Schepper et al., 2014). At that time, the temperatures are estimated to have been 3°C to 6°C higher than modern values in the Western Mediterranean region (Fauquette et al., 2007). In terms of precipitation, a north-south gradient has been identified, with higher than modern precipitation levels in Northwestern Europe and values similar to modern levels in Southwestern Europe (Fauquette et al., 2007). In contrast to the western areas, the climate of the Eastern Mediterranean during the Early Pliocene remains poorly documented.

During the Early-Late Pliocene transition (~3.6 Ma), vegetation patterns in Western Europe, as inferred from numerous pollen records (Suc et al., 1995; Fauquette et al., 2007; Jiménez-Moreno et al., 2010; Combourieu-Nebout et al., 2015; Suc et al., 2018 and references herein), exhibited a clear latitudinal gradient. In Northwestern Europe, a decline in mega-mesothermic taxa (species adapted to persistently humid climates) such as *Engelhardia* and *Taxodium*-type, is evident during the Late Pliocene. In contrast, the Northwestern Mediterranean region still supported mega-mesothermic taxa during the same period, although there was a general increase in deciduous mesothermic (e.g. deciduous *Quercus*) and Mediterranean sclerophyllous taxa (e.g. *Quercus ilex*-type) both better adapted to seasonal dryness. The Southwestern Mediterranean region, however, retained vegetation similar to that of the Early Pliocene, characterized by open, steppe-like landscapes and warm, arid conditions.

Compared to the Western Mediterranean, the Eastern Mediterranean remains poorly documented for this interval, with only a few dated palynological records currently available. Notable examples include a record from the Black Sea (DSDP site 380; Popescu et al., 2010) and another from Ericek in Southwestern Türkiye (Jiménez-Moreno et al., 2015), although the latter captures only the end of the Early Pliocene. Additional pollen records from Anatolia exist, but many are limited by the low sample resolution and chronological control (Yavuz Işık et al., 2011; Alçiçek and Jiménez-Moreno, 2013; Kayseri-Özer et al., 2017; Tuncer et al., 2023; Tagliasacchi et al., 2024a). Despite these limitations, available evidence suggests that prior to 3.6-3.4 Ma, mesothermic forests developed along the Black Sea coast (Popescu et al., 2010), while steppe vegetation prevailed across the Anatolian plateau (Jiménez-Moreno et al., 2015). After 3.4 Ma, both records indicate a transition towards more open landscapes consistent with increasingly arid conditions (Popescu et al., 2010; Jiménez-Moreno et al., 2015). Nonetheless, vegetation and climate dynamics in the Eastern Mediterranean during the Early to Late Pliocene transition, remain poorly constrained due to the scarcity of well-dated high-resolution pollen sequences and complementary proxy data.

The sediment core from Burdur Basin (core BS-87), located in Southwestern Türkiye (ca 30 km west of Acıgöl Basin); previously dated with paleomagnetism by Özkaptan et al. (2018), represents a key record for reconstructing vegetation and climate dynamics in the Eastern Mediterranean region during the Pliocene, as well as for exploring the early development of large pollen grains of Poaceae (proto-cereal). The Eastern Mediterranean is an intriguing area to document the history of this family, a key taxon in Mediterranean vegetation and in a region where the development of agricultural activities emerged from the early Neolithic (Brown et al., 2009; Willcox et al., 2009). Importantly, large Poaceae pollen grains have been recorded on the Anatolian plateau (Acıgöl Basin) during the Pleistocene from 2.3 Ma, with their sizes ranging from 40 to 60 µm and their percentages representing up to 9% of the pollen signal (Andrieu-Ponel et al., 2021). For grains larger than 45-50 µm, Poaceae pollen identification keys assign these grains to domesticated cereals (Andersen, 1979; Tweddle et al., 2005; Joly et al., 2007; Muller et al., 2022). Interestingly, large Poaceae pollen grains exceeding 45–50 µm in size have been identified in Pleistocene deposits, predating the onset of agriculture (Andrieu-Ponel et al., 2021). These have been described by Andrieu-Ponel et al. (2021) as proto-cereals, with their emergence potentially linked to ecological

pressures exerted by large herbivore herds on steppe environments around Acıgöl Basin, possibly driving genetic mutations within Poaceae. Given the complexity of this issue, investigating the presence of proto-cereal-type pollen in other Pliocene and Pleistocene palynological records would be particularly valuable.

Here we propose to address this gap in the Eastern Mediterranean by documenting environmental and climatic changes during the Early-Late Pliocene transition using the Burdur Basin core BS-87. Our specific aims are to:

1) Reconstruct lake dynamics using pollen and Non-Pollen Palynomorphs (NPPs),
2) Reconstruct regional vegetation dynamics based on pollen,
3) Morphologically characterize large pollen grains of Poaceae (*Cerealia*-type),
4) Quantitatively reconstruct climate changes using a multi-method approach, including the Modern Analogue Technique (MAT; Guiot, 1990), Weighted Averaging Partial Least Squares regression (WA-PLS; ter Braak and van Dam, 1989; ter Braak and Juggins, 1993), Random Forest (RF; Prasad et al., 2006), and Boosted Regression Trees (BRT; Salonen et al., 2012) and Climatic Amplitude Method (Fauquette et al., 1998a),
5) Gain a better understanding of regional-scale changes by comparing our results with existing climate reconstructions derived from proxy data and model simulations (PlioMIP2) for the Mediterranean Basin.

2. Study site

2.1 Geographical, geological and hydrological settings

The Anatolian peninsula is defined by a high central plateau (ca. 1000–1200 m a.s.l.), bordered by mountain ranges in the north (the Pontides) and south (the Taurides) (Kuzucuoğlu, 2019). The inner southwestern region of Anatolia, known as the “Lake District” (the Pisidic Lake), contains nine large lakes, and several smaller ones, most of which are tectonic in origin, although some are karstic (Bering, 1971). These lakes are situated at elevations between 850-1100 m a.s.l and are surrounded by mountains with peaks exceeding 2500 m. The region includes lakes with freshwater (Beyşehir and Eğirdir), saline (Akşehir and Burdur) and hypersaline (Acıgöl and Salda) conditions, with the majority classified as endorheic (Kuzucuoğlu, 2019).

Southwest Anatolia (Fig. 1) is defined by three structural units: the basement Bey Dağları autochthon, and the tectonically overlying Antalya and Lycian nappes, which together form the Tauride Orogenic Belt. This orogeny resulted from the closure of the Neotethys Ocean during the Mesozoic to Early Cenozoic (ten Veen et al., 2009). Following the culmination of the Tauride orogeny, the region experienced crustal extension from the Late Miocene onwards, leading to the formation of NE-trending array of normal-fault bounded orogen-top basins that host contemporaneous alluvial-fan, fluvial and lacustrine deposits (Alçiçek et al., 2019).

The Burdur Basin, which contains modern Lake Burdur (37°43'2.748"N, 30°9'14.792"E, 845 m a.s.l.), is one of these orogen-top basins shaped by a NE-trending master-fault and infilled with Late Miocene-Early Pleistocene alluvial-fan, fluvial and lacustrine deposits (Price and Scott, 1991; Alçiçek et al., 2013; Fig. 1). The lake extends approximately 27 km in length and 8 km in width, with an average depth of 60-80 m and a maximum depth of 110 m; anoxic conditions occur in the deepest parts (Çolak et al., 2022). Lake Burdur is an endorheic, alkaline lake with high salinity and elevated ion concentrations, a condition resulting from evaporation exceeding hydrological inputs and leading to the accumulation of dissolved salts and ions (Çolak et al., 2022). Water is supplied primarily by seasonal and perennial rivers (55%), followed by precipitation (40%) and groundwater (5%)

(Çolak et al., 2022; Dervişoğlu et al., 2022). Since 1974, the construction of dams and reservoirs for domestic and agricultural use along nearly all in flowing rivers has led to a 39% reduction in lake volume between 1975 and 2016, this is exacerbated by seasonal drought (Davraz et al., 2019).

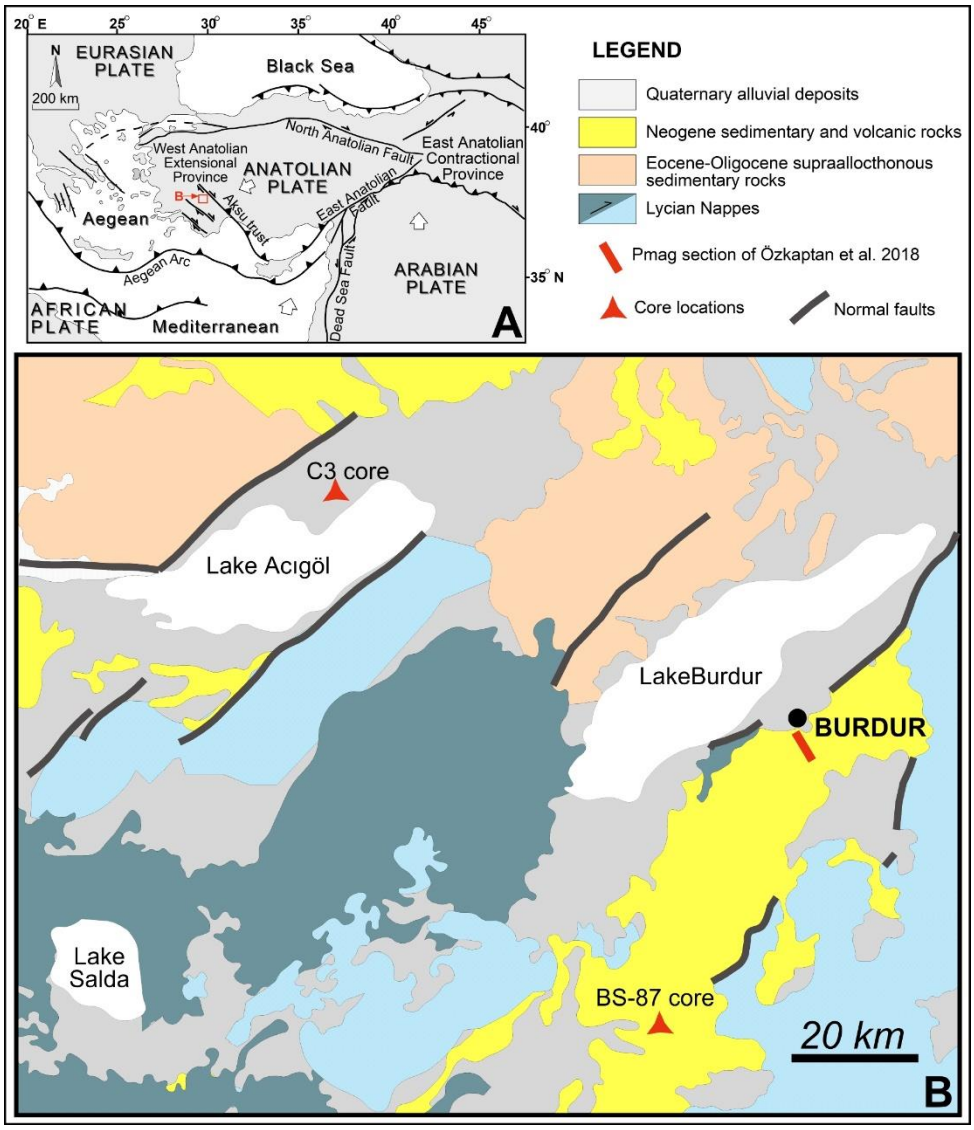

Figure 1: (A) Tectonic map of the Eastern Mediterranean showing major tectonic structures (after Bozkurt, 2003; Alçiçek et al., 2013; Kaymakcı et al., 2018), (B) Geological maps of Acıgöl and Burdur Province and locations of Acıgöl C3 core (Andrieu-Ponel et al., 2021), Burdur Pmag section (Özkaptan et al., 2018a) **and Burdur BS-87 core (this study).**

2.2 Present-day climate and vegetation

The topographic barriers created by the Taurus Mountains block southerly and south-westerly airflows, leading to climate variability, distinct ecological conditions, and a high numbers of endemic species (Medail and Quézel, 1997). The Burdur province is characterized by a Mediterranean climate with hot-dry summers and cool-wet winters according to the Köppen-Geiger climate classification (Kottek et al., 2006). Data from the meteorological station of Burdur (1991-2021) indicates an average annual precipitation of 593 mm, with a maximum in January (80 mm) and a minimum in July (9 mm) and August (8 mm). The mean annual temperature is 12.2°C, with the lowest monthly average in January (1.3 °C) and the highest in July and August (23.7 °C).

Anatolia lies at the intersection of three major floristic regions, the Mediterranean, Euro-Siberian and Irano-Turanian, and hosts one of the richest floras in Europe (Davis et al., 1965). The region is recognized as a biodiversity hotspot and has served as refugium for numerous plant species that were once widespread across Europe and the Mediterranean (Medail and Quézel, 1997; Biltekin et al., 2015). Specifically, Southwest Anatolia marks the boundary between the Mediterranean and Irano-Turanian phytogeographical regions (Davis et al., 1965). The vegetation of this area, particularly within the 'Lake District,' has been extensively catalogued using regional floristic surveys (Pils, 2006). Between 800 and 1200 m a.s.l., vegetation is dominated by evergreen shrubs such as *Quercus coccifera* and *Juniperus excelsa,* along with steppic vegetation composed of xerophytes and chamaephytes (e.g. Poaceae, *Artemisia*, Amaranthaceae). At elevations between 1200 and 1600 m a.s.l., coniferous forests prevail featuring *Juniperus excelsa, J. oxycedrus, Pinus nigra, P. brutia, Cedrus libani*, and *Quercus infectoria*. Above the treeline, around 1600 m a.s.l., alpine meadows dominate, supporting species such as *Astragalus sp.* and *Acantholimon sp.*

3. Material and methods

3.1 Coring, core conservation and stratigraphy

The BS-87 core series from paleo-Lake Burdur was retrieved from Pliocene alluvial fan, fluvial and lacustrine deposits located southeast of the modern lake (Fig. 1). Drilling was conducted at 37°30'59.735"N, 30°7'59.768"E, at an elevation of 1064 m a.s.l. The core is 360 m in length and is currently stored at the warehouse facility of the Mineral Research and Exploration Directorate of Türkiye (MTA) in Ankara. Core sampling was undertaken in 2019 at the MTA warehouse, where one sample was collected every meter in compacted sediment sections.

The stratigraphy of the BS-87 core from Burdur Basin succession has been previously described in several studies (Fig. 2; Sickenberg and Tobien, 1971; Lefevre et al., 1983; Karaman, 1986; Price and Scott, 1991; Saraç, 2003; Platevoet et al., 2008; Alçiçek et al., 2013a, b; Demirel and Mayda, 2014; Alçiçek et al., 2017; Özkaptan et al., 2018; Alçiçek et al., 2019). The core is primarily composed of alternating greenish-grey, yellow-brown, and beige marlstone and siltstone (Fig. 2). Scattered gastropod remains are present at the base of the core (360 m), and at depths of 275 m, 130 m, 80 m, and between 60–20 m. Organic-rich layers are concentrated in the lower part of the sequence, particularly between 325–300 m and 260–210 m. Five coal seams, ranging from dark grey to black color, are observed at approximately 177 m, 130 m, 110 m, 90 m, and 70 m. The top of the core consists of rounded to subrounded gravelstone composed of crystallized limestone.

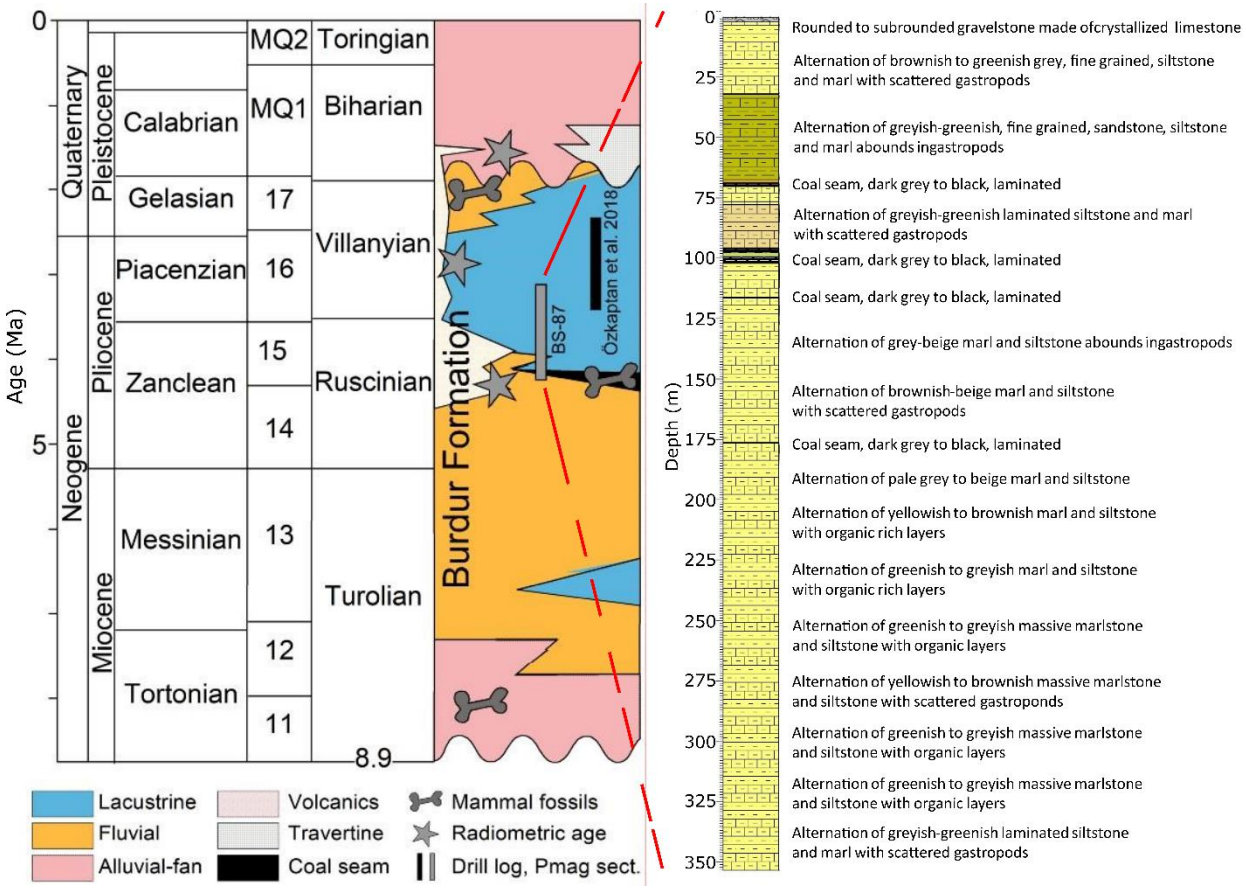

Figure 2. The studied drill-log of BS-87 within the stratigraphy for the Burdur basin-fill succession (Sickenberg and Tobien, 1971; Lefevre et al., 1983; Karaman, 1986; Price and Scott, 1991; Saraç, 2003; Platevoet et al., 2008; Alçiçek et al., 2013a, b; Demirel and Mayda, 2014; Alçiçek et al., 2017; Özkaptan et al., 2018a; Alçiçek et al., 2019). The chronostratigraphic units stand on Hilgen et al. (2012).

3.2 Paleomagnetism and magnetic susceptibility

The time span of the lacustrine and fluvial sedimentary succession of paleo-Lake Burdur, which extends from the late Miocene into the Pliocene, is constrained primarily by mammalian biostratigraphy (zones MN11 to 17; Alçiçek et al., 2019) and palaeomagnetic dating (Özkaptan et al., 2018a). Palaeomagnetic analyses were carried out on full 360 m length of the BS-87 core. Stepwise alternating-field (AF) demagnetization (up to 80 mT) and thermal demagnetization (up to 610°C) of the Natural Remanent Magnetization were performed on 109 and 49 cubic samples (8 cm^3), respectively. Remanent magnetizations were measured using a superconducting rock magnetometer (SRM760R, 2G Enterprises) equipped with an in-line AF demagnetization system, while thermal demagnetization was conducted in a magnetically shielded oven (TD48-SC, ASC). As the core was not azimuthally oriented, the geomagnetic polarity sequence was inferred from the inclination of the Characteristic Remanent Magnetization (ChRM), the stable magnetic signal isolated after progressive demagnetization.

Magnetic susceptibility (MS) was measured on the same samples used for alternating-field (AF) demagnetization of the Natural Remanent Magnetization, which were evenly distributed along the 360 m long BS-87 core. Measurements were conducted using an MFK1 Susceptibility Meter (AGICO) operating at a frequency of 976 Hz and a field strength of 200 A/m.

3.3 Pollen and Non-Pollen Palynomorph (NPP) analyses

Fifty-three samples were collected from the BS-87 core of paleo-Lake Burdur for pollen analysis, spanning from 265 m to the top of the core, with an average sampling resolution of 5 m (ranging from 1.8 m to 15.7 m). For each sample, 15-20 g of sediment was processed following the protocol of Andrieu and Gambin (2025) using Fast-Float heavy liquid (density = 2.0) to separate the minerogenic fraction from palynomorphs. Preparations were mounted on glass slides using glycerol-gelatine jelly. Microscopic analysis was conducted with an Olympus BX53-P microscope at a magnification of 600x. Pollen and NPP taxa were identified using the CEREGE pollen reference collection and published photographic atlases (Beug, 2004; Cugny et al., 2010; Lee et al., 2022; Reille, 1998; Van Geel, 2002).

Pollen of *Pinus sylvestris*-type and *Pinus* mediterranean-type were differentiated based on their grain size, with *P. sylvestris-type* < 66 µm and *P.* mediterranean-type > 66 µm (Reille, 1998). A minimum of 300 pollen grains of terrestrial taxa was counted per slide, excluding aquatic plants (mainly Cyperaceae) and fern spores, in order to obtain a representative assessment of the regional vegetation signal (Lytle and Wahl, 2005). Measurements were conducted on Poaceae pollen grains < 40 µm, focusing on grain diameter (longest axis), annulus and pore dimensions (Joly et al., 2007; Tweddle et al., 2005). Aquatic taxa, fern spores, and NPPs (including algae and fungal spores) were also counted alongside pollen.

Pollen diagrams (Fig. 4) were constructed using the R package *Rioja* (Juggins, 2020) and zoned using CONISS (Grimm, 1987; Juggins, 2020). Principal Component Analysis (PCA) was performed on the pollen and NPP dataset using the *FactoMineR* package in R (version 2.4; Lê et al., 2008).

3.4 Pollen-inferred climate reconstructions

Traditionally, 'Coexistence Approach' methods have been preferred for periods predating the Quaternary because they enable the quantification of climatic conditions during intervals (such as the Pliocene) for which no modern analogs exist in contemporary pollen floras. Among these methods, the Climatic Amplitude Method (CAM), developed by Fauquette et al. (1998a), has proven particularly effective for reconstructing Neogene climate conditions (e.g. Fauquette et al., 1999, 2006; Jiménez-Moreno and Suc, 2007; Jiménez-Moreno et al., 2008). In the present study, CAM has been applied to the Lake Burdur pollen assemblages alongside other methods more commonly used for Quaternary datasets, including the Modern Analog Technique (MAT; Guiot, 1990) and the Weighted Averaging Partial Least Squares regression (WA-PLS; ter Braak and Juggins, 1993) (see also Peyron et al., 1998; Robles et al., 2023; d'Oliveira et al., 2023; Sassoon et al., 2025).

This multi-method approach is made possible by the ecological character of the Burdur Basin, which is dominated by steppe taxa similar to those found in modern Eastern Mediterranean vegetation (Djamali et al., 2009; Robles et al., 2022). Consequently, standard climate reconstruction methods such as MAT and WA-PLS can be reliably applied to the Burdur pollen data, as these assemblages lack relict taxa. By the time of the Early-Late Pliocene transition, most subtropical taxa had disappeared from Southern Europe, replaced by sclerophyllous Mediterranean ecosystems (Suc, 1984; Combourieu-Nebout et al., 2015; Suc et al., 2018). A multi-method strategy increases the robustness and reliability of climate reconstructions, particularly when compared to approaches relying on a single technique (Brewer et al., 2008; Peyron et al., 2005, 2011, 2013; Salonen et al., 2019).

In this study, five methods were selected: Climatic Amplitude Method (CAM, Fauquette et al., 1998a, b), the Modern Analog Technique (MAT; Guiot, 1990), the Weighted Averaging Partial Least Squares regression (WA-PLS; ter Braak and van Dam, 1989; ter Braak and Juggins, 1993), the Random Forest (RF; Prasad et al., 2006) and the Boosted Regression Trees (BRT; Salonen et al., 2012). RF and BRT are machine learning algorithms

based on regression trees models trained on ecological data, and have recently been applied to paleoclimatic reconstruction across both Northern Europe (Salonen et al., 2019, 2024) and the Mediterranean Basin (Robles et al., 2023; d'Oliveira et al., 2023; Charton et al., 2025; Sassoon et al., 2025).

All the climatic reconstruction methods applied in this study require a modern pollen calibration dataset. For the MAT, WA-PLS, RF and BRT, we use a subset of the Eurasian/Mediterranean modern pollen dataset (n = 3373 sites) originally compiled by Peyron et al. (2013, 2017) and subsequently expanded by Dugerdil et al. (2021a) and Robles et al. (2022, 2023). A geographical filter was applied to select modern samples from Western Europe (11°W) to Türkmenistan (58°E) and Central Europe (51°N) to North Africa (29°N). After applying these constraints, the final calibration dataset consisted of 1776 modern pollen samples.

These samples represent six biomes: "Cool Mixed Forest" (COMX), "Cool Steppe" (COST), "Temperate Deciduous Forest" (TEDE), "Warm Mixed Forest" (WAMX), "Warm Steppe" (WAST), and "Xerophytic Wood/Shrub" (XERO). The performance of each reconstruction method and the suitability of the calibration dataset were statistically evaluated following Dugerdil et al. (2021a) using Root Mean Square Error (RMSE) and the coefficient of determination (R^2) as presented in the Supplementary Table S1.

For CAM, the calibration dataset comprises over 8000 modern pollen records for the Northern Hemisphere. Climate estimate are expressed as a climatic range and a "most likely value", corresponding to a weighted mean. This statistical approach has been tested on modern pollen datasets, and its performance (R^2 and RMSE) is also reported in Supplementary Table S1.

Six climate parameters were reconstructed: mean annual air temperature (MAAT), mean temperature of the warmest month (MTWA), mean temperature of the coldest month (MTCO), mean annual precipitation (PANN), mean winter precipitation (Pwinter; December-February) and mean summer precipitation (Psummer; June-August). Precipitation seasonality is not reconstructed using the Climatic Amplitude Method (CAM). For each parameter, the methods with the highest R^2 and the lowest RMSE were selected for interpretation.

In the Burdur dataset, Cyperaceae and ferns were excluded due to their strong association with local, rather than regional, vegetation dynamics. For CAM, *Pinus* and unidentified Pinaceae taxa were also excluded from the pollen sum, due to poor preservation of bisaccate pollen grains following Fauquette et al. (1998b, 1999).

The WA-PLS and MAT methods were applied using the R package *Rioja* (Juggins, 2020), RF using *the randomForest* package (Liaw and Wiener, 2002), and BRT using the *dismo* package (Hijmans et al., 2021).

4. Results

4.1 Age-depth model

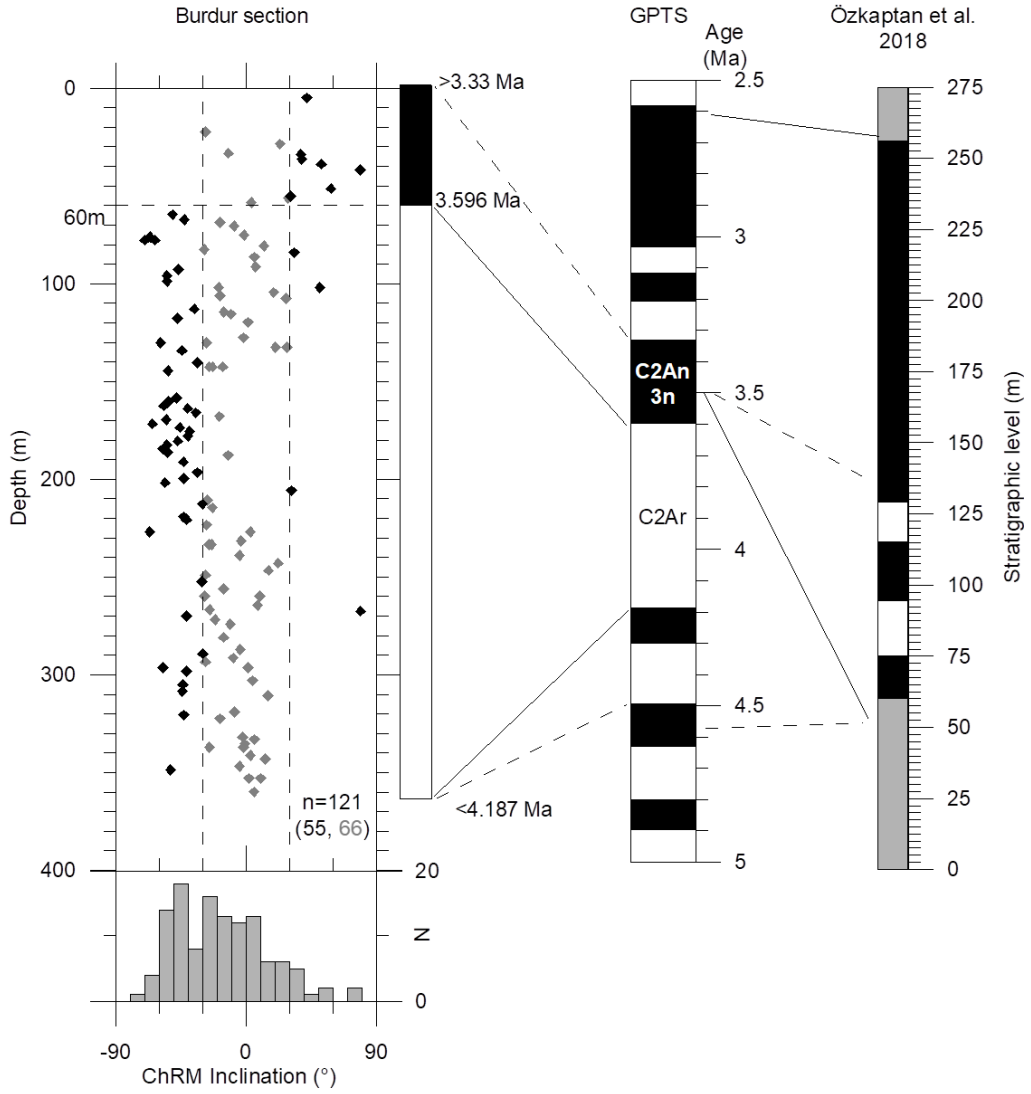

Figure 3: Magnetostratigraphic correlations of the Burdur Pliocene lacustrine sediment in BS-87 core (this study; left) compared to the previously published surface section of Burdur (Özkaptan et al. 2018) with the GPTS (Hilgen et al., 2012). ChRM: Characteristic Remanent Magnetizations. Absolute values of inclination above or below 30° are shown as black and grey symbols, respectively.

Normal and reverse polarities were determined based on the inclination of the Characteristic Remanent Magnetization ChRM directions (Fig. 3). Due to varying levels of overprint, intermediate inclinations (absolute values <30°), represented by grey diamonds, were considered only as supporting data, while black diamonds indicate reliable polarity determinations. The entire core below 60 m depth is characterized predominantly by reverse polarity. We have not attempted to identify short normal chrons within this interval, as the presence of four isolated normal samples (I>30°) could result from sporadic orientation errors (e.g., upside down readings) or issues related to demagnetization. It is standard practice in magnetostratigraphy not to interpret isolated opposite polarity samples as reliable magnetic field records.

Above 60 m, a well-defined interval of polarity is observed. In comparison to the predominantly normal polarity stratigraphy documented approximately 20 km north of the study site (Özkaptan et al., 2018; Fig.1), the

most plausible interpretation is that the long reverse chron in our record corresponds to Chron C2Ar. This correlation implies that the Burdur core lies stratigraphically below the northern section, with a minor overlap likely within the C2An3n normal chron. This interpretation will be further expanded on in the discussion section.

335

4.2 Pollen and Non-Pollen Palynomorphs (NPPs)

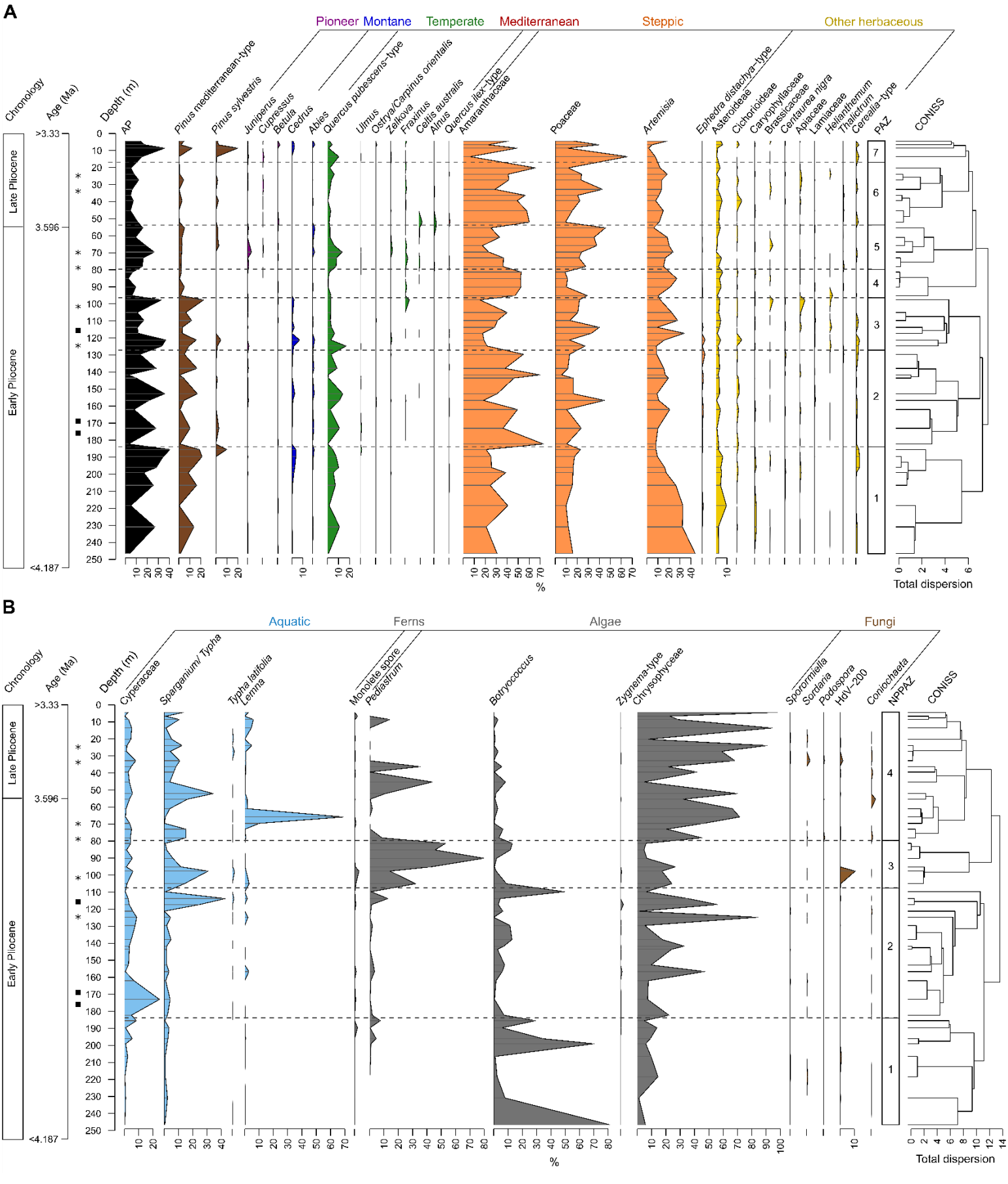

Figure 4: Synthetic pollen diagrams from Burdur Basin (Türkiye) against core depth. A) Selected terrestrial pollen taxa, expressed as percentages of total terrestrial pollen. AP: Arboreal Pollen. PAZ: Pollen Assemblage Zones. B) Selected hygrophilous and aquatic pollen taxa and NPPs. Aquatic pollen taxa are expressed in percentages of total pollen. Fern spores, algae and fungi are expressed in percentages of total terrestrial pollen and NPPs. NPPAZ: Non-Pollen Palynomorph Assemblage Zones. Black rectangles indicate levels with macroscopic charcoal or wood. Black stars indicate very organic levels with shells.

Table 1: Description of arboreal, herbaceous, hygrophilous pollen and Non-Pollen Palynomorphs (NPPs) of Burdur core against depth and age. Values represent the mean percentages for each PAZ (Pollen Assemblage Zone); NPPAZ: Non-Pollen Palynomorph Assemblage Zones. AP: Arboreal Pollen.

	Age (Ma)	Depth (m)	PAZ	Total of AP %	Herbaceous pollen types (HPT) Arboreal pollen types (APT)	NPPAZ	Hygrophilous pollen NPPs
Late Pliocene	<4.187	17-4	7	21	HPT: Poaceae (33%), Amaranthaceae (21%), *Artemisia* (8%) APT: *Pinus* mediterranean-type, *P. sylvestris, Quercus pubescens*-type, *Cedrus*	4	Semi-aquatic: Chrysophyceae (well-developed vegetation) Green algae: *Pediastrum* (~45 m and ~10 m), *Lemna* (~65 m), low *Botryococcus* Fungal spores: *Sordaria, Podospora*, Coniochaeta
		54-17	6	6	HPT: Amaranthaceae (50%), Poaceae (21%), *Artemisia* (13%)		
Early Pliocene	3.596	80-54	5	17	HPT: Poaceae (32%), Amaranthaceae (29%), Artemisia (17%) APT: *Quercus pubescens*-type, *Pinus* mediterranean-type, *P. sylvestris, Juniperus, Abies, Zelkova, Fraxinus*		
		96-89	4	6	HPT: Amaranthaceae (51%), *Artemisia* (19%), Poaceae (15%)	3	Green algae: *Pediastrum, Botryococcus* Semi-aquatic: *Sparganium/Typha*, Chrysophyceae Fungal peak: type HdV-200 at 100m
		127-96	3	22	HPT: Amaranthaceae (25%), Poaceae (24%), *Artemisia* (13%) APT: *Pinus* mediterranean-type, *Quercus pubescens*-type, *Cedrus*		
		182-127	2	17	HPT: Amaranthaceae (46%), Poaceae (17%), *Artemisia* (13%) APT: Decline of *Pinus* mediterranean-type	2	Golden algae: Chrysophyceae Semi-aquatic: Cyperaceae at start, *Sparganium/Typha* at end Green algae: *Botryococcus* decreases then increases Macroscopic charcoal or wood present
	>3.33	247-184	1	23	HPT: Amaranthaceae (28%), *Artemisia* (23%), Poaceae (16%) APT: Maximum arboreal taxa (*Pinus* mediterranean-type, *Quercus pubescens*-type)	1	Green algae: *Botryococcus* Golden algae: Chrysophyceae Semi-aquatic: Cyperaceae, *Sparganium/Typha*

Terrestrial vegetation changes

Of the 53 samples analyzed from the Burdur Basin, 46 were polliniferous and 7 were sterile; yielding a total of 69 identified terrestrial pollen taxa. Throughout the sequence, the terrestrial pollen assemblages reflect open-ground vegetation dominated by steppe taxa, particularly Amaranthaceae (ca. 37%), Poaceae (ca. 22%), and *Artemisia* (ca. 16%). The pollen diagram (Fig. 4A) is divided into seven pollen assemblage zones (PAZ) based on the CONISS clustering method (Grimm, 1987; Table 1). A major boundary is observed at 100 cm depth, separating PAZ 1 to 3, characterized by more arboreal pollen (ca. 20%), from PAZ 4 to 6, which exhibit a reduced arboreal pollen count (ca. 10%) largely due to decreases in *Pinus* and *Quercus*.

The composition of steppe taxa varies through time, alternating between zones dominated by Amaranthaceae (PAZ 1, 2, 4, 6) and those where Poaceae are more prominent (PAZ 3, 5, 7). Periods dominated by Poaceae are also marked by increases in arboreal taxa, particularly due to a rise in *Quercus pubescens*-type pollen.

PAZ 1 (247-184 m) records an open steppic vegetation dominated by Amaranthaceae (ca. 28%), *Artemisia* (ca. 23%), and Poaceae (ca. 16%), with a relatively low percentage of trees (ca. 23%), including *Pinus* mediterranean-type and *Quercus pubescens*-type. Rare pollen types (< 5%) include: Asteroideae, Caryophyllaceae, *Cedrus*, and *Pinus sylvestris*-type.

PAZ 2 (184-127 m) shows a dominance of Amaranthaceae (ca. 46%), a decrease of *Artemisia* (ca. 13%), whereas Poaceae remain constant (ca. 17%). Arboreal pollen taxa also decrease slightly (17%), notably due to the decline of *Pinus* mediterranean-type. Rare pollen types include: Asteroideae, Cichorioideae, *Cerealia*-type, *Pinus sylvestris*-type, *Ephedra distachya*-type, *Cedrus,* and *Abies*.

PAZ 3 (127-96 m) is marked by an increase of Poaceae (ca. 24%) and *Artemisia* (ca. 13%) and a decrease of Amaranthaceae (ca. 25%). Arboreal pollen taxa increase slightly again (ca. 22%) due to the rise of *Pinus* mediterranean-type and *Cedrus*. Rare pollen types include: Asteroideae, *Cerealia*-type, Apiaceae, Cichorioideae, *Helianthemum*, *Pinus sylvestris*-type, and *Cedrus*.

PAZ 4 (96-80 m) is characterized by the net increase of Amaranthaceae (ca. 51%) and *Artemisia* (19%), while Poaceae (15%) and arboreal pollen (ca. 6%) decrease drastically. Rare pollen types include: Asteroideae, *Pinus* mediterranean-type*, Quercus pubescens*-type, and *Helianthemum*.

PAZ 5 (80-54 m) is defined by an increase of Poaceae (ca. 32%) and arboreal pollen taxa (ca. 17%), the decrease of Amaranthaceae (ca. 29%), while *Artemisia* remains constant (ca. 17%). The arboreal pollen taxa diversify with the presence of *Quercus pubescens*-type, *Pinus* mediterranean-type*, P. sylvestris*, *Juniperus, Abies, Zelkova*, and *Fraxinus*. Rare herbaceous pollen types include Asteroideae and Brassicaceae.

PAZ 6 (54-17 m) is marked, as with PAZ 4, by an increase of Amaranthaceae (ca. 50%) while Poaceae (ca. 21%), *Artemisia* (13%), and arboreal pollen (ca. 6%) decrease. Rare pollen types include: Asteroideae, *Quercus pubescens*-type, *Pinus* mediterranean-type, Cichorioideae, and Apiaceae.

PAZ 7 (17-4 m) is characterized by an increase of Poaceae (ca. 33%) and arboreal pollen taxa (ca. 21%), whereas Amaranthaceae (ca. 21%) and *Artemisia* (ca. 8%) decrease. Arboreal pollen taxa include *Pinus* mediterranean-type*, P. sylvestris, Quercus pubescens*-type, and *Cedrus*. Rare herbaceous pollen types include Asteroideae and *Cerealia*-type.

Hygrophilous vegetation, fungi and algae

The diagram for Non-Pollen Palynomorphs (NPPs) and hygrophilous vegetation is divided into four NPP assemblage zones (NPPAZ) as defined using the CONISS clustering method (Fig. 4B, Table 1).

NPPAZ 1 (247-184 m) is characterized by three major peaks of the green algae *Botryococcus*, the presence of the golden algae Chrysophyceae, and semi-aquatic vegetation composed of Cyperaceae and *Sparganium/Typha.*

NPPAZ 2 (184-107 m) records an increase of Chrysophyceae and semi-aquatic vegetation with Cyperaceae and *Sparganium/Typha*, whereas *Botryococcus* decreases. This zone is also marked by a high percentage of Cyperaceae at the beginning and a high percentage of *Sparganium/Typha* at the end, accompanied by the presence of macroscopic charcoal or wood in the sediment. The transition to NPPAZ 3 is marked by a large peak of *Botryococcus*.

NPPAZ 3 (107-80 m) is distinguished by a significant proportion of the green algae *Pediastrum* accompanied by *Botryococcus*, a rich semi-aquatic vegetation mainly composed of *Sparganium/Typha*, and the presence of Chrysophyceae. A peak of the fungi of type HdV-200 is recorded around 100 m.

NPPAZ 4 (80-4 m) is mainly characterized by a large proportion of Chrysophyceae and well-developed semi-aquatic vegetation. However, this zone is punctuated by two peaks of *Pediastrum* (~45 m and ~10 m) and a peak of *Lemna* (~65 m). The proportion of *Botryococcus* is low, and some fungal spores are recorded (*Sordaria, Podospora*, Coniochaeta).

Principal Component Analysis (PCA)

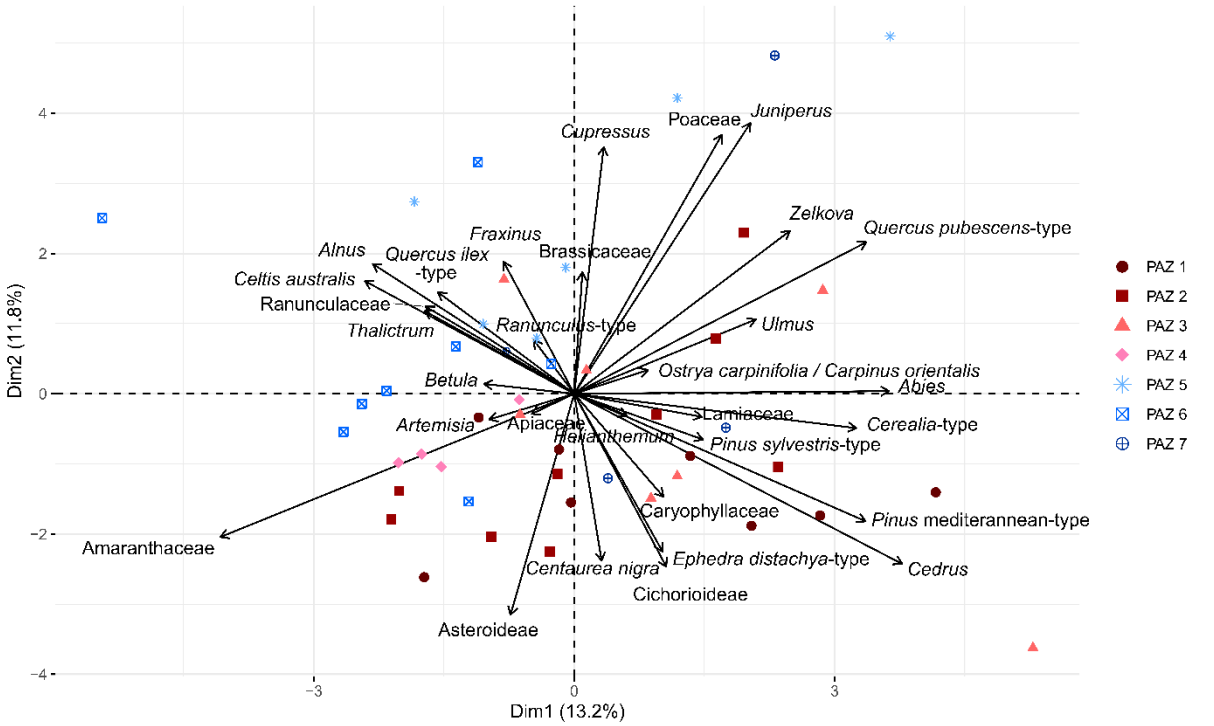

Figure 5: Principal Component Analysis (PCA) on selected terrestrial pollen taxa from the core BS-87 from Burdur Basin succession. The sample map was color-coded according to the PAZ (presented in Fig. 4).

Principal Component Analysis (PCA) was performed on selected terrestrial pollen taxa (Fig. 5), with the sample scores color-coded according to the pollen assemblage zones (PAZ) defined by the CONISS method (Fig. 4A). The first two principal components (PCA axis 1 and PCA axis 2) account for 25% of the total variance, 13.2% and 11.8% respectively.

PCA axis 1 distinguishes samples dominated by open vegetation taxa (Amaranthaceae, *Artemisia*, Asteroideae) and riverine elements (*Fraxinus, Alnus*, Ranunculaceae) from those with higher proportions of arboreal or shrub taxa, such as *Quercus pubescens*-type, *Juniperus, Pinus, Cedrus, Ephedra distachya*-type). Samples from PAZ 4, 5, 6 have negative scores on Axis 1 and are generally associated with open vegetation, with the except of two samples in PAZ 5 (at 69.6 m and 65.85 m), where arboreal pollen becomes more prominent. Conversely, samples from PAZ 1, 3, and 7 exhibit positive scores and are associated with more developed arboreal and shrub vegetation.

PCA Axis 2 separates samples dominated by steppic taxa (Amaranthaceae, Asteroideae, Cichorioideae, *Ephedra distachya*-type) from those characterized by deciduous arboreal taxa (*Quercus pubescens*-type, *Fraxinus, Alnus, Zelkova, Ulmus, Ostrya carpinifolia/Carpinus orientalis*) and herbaceous taxa such as Poaceae and Ranunculaceae. Samples from PAZ 1, 2, and 4 show negative values on Axis 2 and are associated with steppic vegetation, while samples from PAZ 5 have positive values and are linked to a greater representation of deciduous arboreal taxa.

Large pollen grains of Poaceae

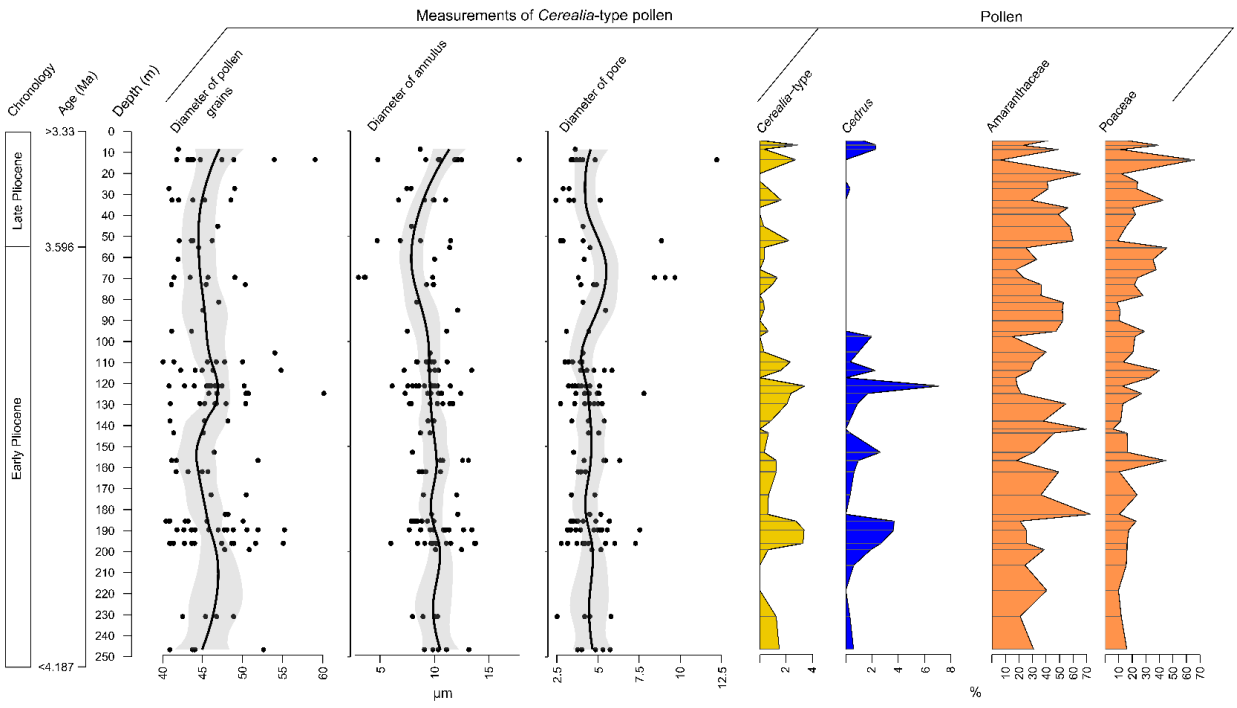

Figure 6: Measurements of diameter of pollen grains, annulus and pores of large pollen grains of Poaceae from the core BS-87 from Burdur Basin against core depth. The measurements are compared with the variation in the percentages of some of the more characteristic pollen taxa, i.e. *Cerealia*-type, *Cedrus*, Amaranthaceae and Poaceae.

A total of 133 large Poaceae pollen grains (>40 µm in diameter), were identified and measured throughout the sequence (Fig. 6; Supplementary Table S2). Measurements yielded a mean grain diameter of 45.8 ± 3.9 µm, a

mean annulus diameter of 9.7 ± 2.1 µm, and a mean pore diameter of 4.5 ± 1.4 µm. Large Poaceae grains are most abundant towards the end of PAZ 1 (200-185 m), at the end of PAZ 2, and throughout PAZ 3 (130-100 m).

Although considerable variability was observed within individual samples, no consistent trend in grain size was detected along the sequence. Correlation analysis indicates a weak but statistically significant positive relationship between grain diameter and annulus diameter ($r = 0.22$; $p \leq 0.05$), while no significant correlation was found between pollen grain diameter and pore size (Supplementary Figure S1).

4.3 Pollen-inferred climate reconstructions

Pollen-inferred climate reconstructions based on the five selected methods are presented in Figure 7. Model performance statistics indicate that the BRT method yields the highest accuracy, with the best R^2 and RMSE values (Supplementary Table S1). Among the tested approaches, MAT, BRT and WA-PLS appear to be sensitive methods, unlike the RF method (Fig. 7). CAM also shows lower sensitivity; however, it differs methodologically, as it provides a climatic range along with a "most likely value" derived from a weighted mean. The full range of CAM-derived climatic interval is provided in Supplementary Table S3.

Reconstructed mean annual temperatures (MAAT) are generally close to modern values using WA-PLS across all the PAZs (1–7). CAM reconstructs slightly warmer-than-modern conditions in PAZ 1–3, followed by values similar to present in PAZ 4–7. In contrast, BRT and RF consistently yield cooler-than-modern MAAT throughout the sequence, while MAT reconstructs near-modern temperatures in PAZ 1–3, shifting to becoming cooler conditions in PAZ 5–7. The reconstructed mean temperature of the warmest month (MTWA) shows a similar pattern to MAAT, except for MAT, which infers warmer-than-modern conditions, and BRT, which reconstructs values similar to today.

For the mean temperature of the coldest month (MTCO), all five methods indicate colder conditions relative to the present, with MAT, BRT, and RF showing the strongest deviations. Notably, temperature trends reconstructed by CAM occasionally diverge from those of the other methods.

Mean annual precipitation (PANN) is reconstructed as close to modern values by CAM and RF, but significantly lower by WA-PLS, BRT and especially MAT. Seasonal precipitation reconstructions suggest higher summer precipitation than present, particularly in the RF model, and lower winter precipitation across most methods. Overall, CAM reveals limited climatic variability over time, whereas MAT indicates greater temporal fluctuations.

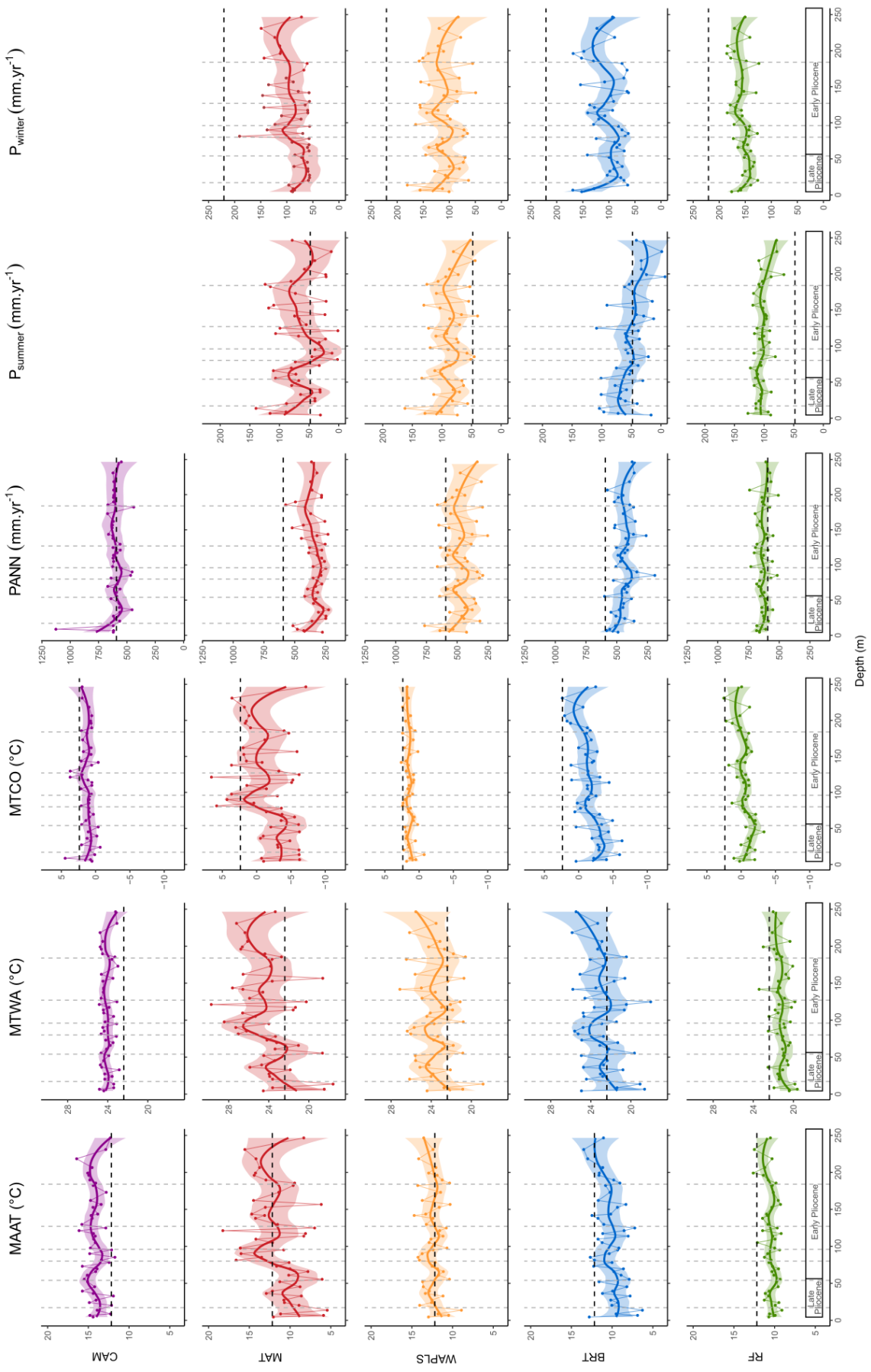
MAAT (°C)
MTWA (°C)
MTCO (°C)
PANN (mm.yr-1)
Psummer (mm.yr-1)
Pwinter (mm.yr-1)
CAM
MAT
WAPLS
BRT
RF
Late Pliocene
Early Pliocene
Depth (m)

Figure 7: Burdur Basin pollen-inferred climate reconstruction based on five methods against depth: CAM (Climatic Amplitude Method), MAT (Modern Analogue Technique), WA-PLS (Weighted Averaging Partial Least Squares regression), BRT (Boosted Regression Trees) and RF (Random Forest). Large lines correspond to loess smoothed curves and shaded areas to the 95 % confidence interval. Black dashed lines correspond to modern climate values of Burdur. Grey dashed lines correspond to Pollen Assemblage Zones (Fig. 4A). MAAT: mean annual temperature. MTWA: mean temperature of the warmest month. MTCO: mean temperature of the coldest month. PANN: mean annual precipitation. Psummer: summer precipitation. Pwinter: winter precipitation.

5. Discussion

5.1 Age-depth model

The proposed magnetostratigraphic framework establishes a single tie point at 3.596 Ma, corresponding to 60 m depth, and constrains the age of the core between >3.33 Ma at the top and <4.19 Ma at the base. This places the entire sequence within the Pliocene and identifies the Early-Late Pliocene transition at 60 m depth (Fig. 3). This magnetostratigraphic solution, although not unique in the absence of independent chronological constraints within the core, is consistent with the regional biostratigraphic constraints of the Burdur sedimentary sequence (mammalian zones reported in 3.2 and paleomagnetic study of Özkaptan et al., 2018). Based on this interpretation, the estimated sedimentation rate exceeds 51 cm/ka in the lower part of the core (below 60 m) and 22 cm/ka in the upper section. These rates are consistent with regional variability and are higher than the >18 cm/ka sedimentation rate inferred approximately 20 km to the north in a more recent study by Özkaptan et al. (2018). Given known geographic and temporal variability in sedimentation patterns within the Burdur Basin, this discrepancy seems plausible. Alternative correlations of the 60-360 m long reversed polarity interval with the younger magnetozones proposed by Özkaptan et al. (2018) would imply sedimentation rate four to five times higher than observed, which are considered unrealistic. A lower sedimentation rate for the reversed chron below 60 m depth could be obtained by assuming that the short normal chron below 4.19 Ma was missed, thereby placing the base of the studied section above 4.5 Ma. This adjustment would yield a sedimentation rate of ~31cm/ka rather than 51 cm/ka. However, this assumption does not improve the fit with the mammal zonation (Fig.2), and remains poorly unconstrained.

The age of the polarity transition at 3.596 Ma has a precision well below 10 ka, since this transition corresponds to the base of the Piacenzian, which is so well characterized that it is the subject of a golden spike in the chronostratigraphic scale (Gradstein and Ogg, 2020). However, the depth chosen for the 3.596 Ma tie point has an uncertainty of about 10 m, depending on sampling interval and the sharpness of the polarity change. This corresponds to a maximum age uncertainty of about 44 ka, based on the lower estimate of sedimentation rate. With an average sampling resolution of one meter (on average), the temporal resolution of the dataset falls within the range of approximately 2-4 ka between samples. This resolution is insufficient for resolving short-term environmental cyclicities of ~20 ka, such as those detected in the magnetic susceptibility record, which would require 5 to 10 samples per cycle for reliable analysis.

5.2 Vegetation changes and plant diversity around the Mediterranean Basin during the Early-Late Pliocene transition

Dynamic of Burdur sequence

The stratigraphy of the Burdur sequence reveals an alternation between marlstone and siltstone units (Fig. 2), suggesting shifts between calm depositional phases and more dynamic episodes. Marlstone, composed of fine-grained, carbonate-rich deposits, typically forms under calm, shallow, or stagnant waters conditions. In contrast, siltstone reflects enhanced siliciclastic input, generally associated with increased runoff or erosion. This lithological alternation likely reflects cyclical climatic variations influencing the hydrodynamics of the basin.

Pollen of hygrophilous plants and algae provide further insight into lake's trophic status over time. During the Early Pliocene (NPPAZ 1), the record is marked by three distinct peaks of the planktonic colonial green algae *Botryococcus,* alongside presence of planktonic golden-brown algae (Chrysophyceae), and limited semi-aquatic vegetation (Cyperaceae and *Sparganium/Typha)* (Fig. 4B). *Botryococcus* is typically found in freshwater environments such as fens, temporary pools, ponds and lakes, but also tolerates moderate salinity (Van Geel, 2002). *Botryococcus braunii,* the dominate species in the Burdur sequence, can tolerate salinities up to 8‰ (Matthiessen and Brenner, 1996) and is known to bloom following freshwater input in slightly saline lakes, such as those in Australia (Wake and Hillen, 1980). This genus is ecologically versatile and occurs in oligotrophic, mesotrophic or eutrophic conditions (Komárek and Marvan, 1992; Jankovská and Komárek, 2000). However, its dominance, combined with the absence or very occurrence of other green algae, may point to relatively extreme environments, often characterized by very cold, clear, oligotrophic, and possibly dystrophic conditions (Jankovská and Komárek, 2000). Chrysophyceae are typically found in humic, neutral to slightly acidic lakes and ponds, and are most common under oligotrophic, and occasionally mesotrophic to eutrophic, conditions (Kristiansen and Škaloud, 2017; Smol, 1988; Tolotti et al., 2003). In the Burdur record, the poor development of semi-aquatic vegetation, the presence of the algae *Botryococcus* and Chrysophyceae, and the absence of other green algae collectively suggest oligotrophic conditions during NPPAZ 1.

In NPPAZ 2, *Botryococcus* abundance decreases, while Chrysophyceae and semi-aquatic taxa (Cyperaceae and *Sparganium/Typha*) increase slightly (Fig. 4B). The shift suggests a transition towards oligotrophic or mesotrophic conditions. The presence of mollusk shells in this interval (Fig. 4B) further supports the interpretation of improved trophic conditions, typically associated with such nutrient levels.

The transition from the end of the Early Pliocene to the beginning of the Late Pliocene is marked by alternating trophic conditions in Burdur Basin, as indicated in NPPAZ 3 and 4 (Fig. 4B). Three intervals (~110-80 m, ~55-30 m, ~10 m) are characterized by the presence of the planktonic colonial green algae *Pediastrum,* often accompanied by *Botryococcus*, semi-aquatic vegetation (Cyperaceae, *Sparganium/Typha*) and the presence of Chrysophyceae algae. *Pediastrum,* typically found in freshwater fens, temporary pools, ponds and lakes, can also tolerate saline environments (Komárek and Jankovská, 2001; Van Geel, 2002). *Pediatrum boryanum,* the most abundant species in the Burdur sequence, is known to tolerates salinities up to 8% (Matthiessen and Brenner, 1996) and is particularly common in hard-water eutrophic lakes (Van Geel, 2002). The co-occurrence of *Botryococcus*, *Pediastrum* and Chrysophyceae suggests mesotrophic or eutrophic conditions during this interval.

In contrast, two periods (~80-55 m, ~30-15 m) are dominated by Chrysophyceae, alongside semi-aquatic vegetation (Cyperaceae, *Sparganium/Typha)* and a notable peak of *Lemna* at ~65 m. *Lemna* is a free-floating

aquatic plant, whose rapid biomass increase can contribute to lake eutrophication (Gostyńska et al., 2022). The assemblage of Chrysophyceae, *Lemna* and semi-aquatic and aquatic taxa in these intervals suggests mesotrophic conditions between 80 and 55 m and oligotrophic or mesotrophic conditions between 30 and 15 m. The occurrence of mollusk shells (Fig. 4B) further supports an interpretation of oligotrophic to mesotrophic conditions during these phases.

Characterization of large Poaceae pollen grains and comparison with other pollen records of Burdur Basin

Large Poaceae pollen grains are recorded in the Burdur sequence, but their relative abundance is lower than at Acıgöl Basin, where values reach up to 9% (Andrieu-Ponel et al., 2021); in contrast the Burdur record does not exceed 3.5% (Fig. 6). Morphologically, these large Poaceae grains resemble those of domesticated cereals found in recent periods. However, a clear distinction between wild and domesticated forms cannot be made based solely on morphology. Modern identification keys define domesticated Poaceae pollen by grain diameter of 37-47 µm, annulus diameter of 8-11 µm, and pore diameter of 3-4 µm (Andersen, 1979; Beug, 2004; Tweddle et al., 2005; Joly et al., 2007). Measurements from Burdur exceed these ranges, often on at least two parameters, as outlined by Andersen (1979) and Joly et al. (2007) but remain insufficient for definitive taxonomic classification. The challenge of distinguishing domesticated from wild Poaceae pollen is further complicated by the presence of the genus *Lygeum* in some Mediterranean Pliocene records (Bessais and Cravatte, 1988). *Lygeum spartum,* a species typical of semi-arid Mediterranean environments, produces pollen with an elongated shape, large grain diameter (~80 µm), and prominent annulus (Reille, 1998). However, *Lygeum* pollen has not been identified in the Burdur sequence.

Statistical analysis reveals that high proportions of large Poaceae pollen are significantly positively correlated with *Cedrus* ($r = 0.60$, $p \leq 0.05$) and negatively correlated with Amaranthaceae ($r = -0.41$, $p \leq 0.05$) (Fig. 6; Supplementary Figure S1). *Cedrus* is generally associated with cool to cold climatic conditions (Magri and Parra, 2002; Quézel and Médail, 2003; Jiménez-Moreno et al., 2020; Xiao et al., 2022), whereas Amaranthaceae is indicative of semi-desert vegetation (e.g. Zheng et al., 2014; Robles et al., 2022). These results suggest that large Poaceae pollen grains are more abundant during cooler periods, as indicated by their positive correlation with *Cedrus*, and less frequent during drier phases, as shown by their negative correlation with Amaranthaceae.

To explain the presence of proto-cereal-type pollen, Andrieu-Ponel et al. (2021) proposed several hypotheses, including selective pressure from large herbivore herds on steppe ecosystems (Spengler et al., 2021; Malhi et al., 2022) and the emergence of polyploidy in Poaceae species under drought conditions (Manzaneda et al., 2012). However, unlike Acıgöl, the Burdur record shows a low abundance of coprophilous fungal spores, and lacks vegetation indicators of arid conditions during intervals with large Poaceae pollen (Fig. 4, 6). This suggests that the biological perturbations proposed for Acıgöl may not apply directly to Burdur, or may have operated under different environmental constraints. Further targeted research on the size distribution of large Poaceae pollen grains at Acıgöl is needed to better clarify the relationship between their morphology and climate variability.

Steppe vegetation in Southwestern Anatolia

The Early Pliocene pollen record for Burdur sequence (PAZ 1) is dominated by steppe taxa, including *Artemisia,* Amaranthaceae and Poaceae, alongside a moderate arboreal signal represented by *Quercus pubescens*-type and *Pinus* mediterranean-type (Fig. 4A). Pollen samples from this interval exhibit positive values on Axis 1

and negative values on Axis 2 of PCA, indicating a mixed vegetation pattern combining arboreal and steppe elements (Fig. 5). The proportion of *Artemisia* is especially high at the base of the sequence. This genus is a well-established indicator of semi-desert steppe environments (Dugerdil et al., 2021b; Robles et al., 2022; Zhao et al., 2022). Notably, pollen percentage of *Artemisia* exceeding 30%, corresponds to at least 5% cover in the local vegetation (Zhao et al., 2022). Today, such *Artemisia*-dominated steppe vegetation is found in regions such as Syria (El-Moslimany, 1990), Jordan (Davies and Fall, 2001), Iran (Djamali et al., 2009), China (e.g. Zhao and Herzschuh, 2009; Xu et al., 2009; Li et al., 2011; Zhang et al., 2018; Zhao et al., 2022), and Mongolia (Ma et al., 2008; Dugerdil et al., 2021a). The arboreal component in the Burdur record includes *Quercus pubescens*-type (6%) and *Pinus* mediterranean-type (12%), both of which are prolific pollen producers adapted to wind dispersal (Connor et al., 2004). These taxa are capable of long distance transport, even across complex topography (Ramezani, 2013; Robles et al., 2022). In large sedimentation basins like Burdur, Pinaceae pollen may be transported via river systems from higher elevations (Suc et al., 2018). Furthermore, *Quercus pubescens*-type pollen can reach up to 15% of the total pollen sum even in the absence of trees in the catchment areas (Robles et al., 2022). Thus, the arboreal pollen signal in the Burdur record is best interpreted as reflecting regional vegetation dynamics rather than local woodland. Towards the end of the Early Pliocene interval, *Cedrus* pollen appears in conjunction with large Poaceae pollen grains. *Cedrus* occurs across a broad ecological range, from semi-arid to humid zones, but it is particularly adapted to cool to cold climates (Magri and Parra, 2002; Quézel and Médail, 2003; Jiménez-Moreno et al., 2020; Xiao et al., 2022). It is a good wind disperser and today is primarily found at mid to high elevations (~1500-2500 m.a.s.l.) in the Mediterranean mountains of North Africa (Rif and Atlas Mountains) and in the Middle East (Türkiye, Syria, Lebanon) (Quézel and Médail, 2003). We interpret the *Cedrus* pollen at Burdur as a regional signal, most likely originating from the surrounding mountains of Southwestern Anatolia.

In PAZ 2 (Fig. 4A), the vegetation continues to be dominated by steppe taxa, including Amaranthaceae, *Artemisia*, Poaceae and *Ephedra distachya*-type, while the representation of arboreal taxa remains stable. This composition is reflected in the PCA results, where negative values on Axis 2, consistent with steppic vegetation (Fig. 5). The proportation of Amaranthaceae in this interval is particularly high, reaching up to 46%. This taxon is widespread in semi-arid regions, where it can comprise 30- 80% of the pollen signal (Connor et al., 2004; Robles et al., 2022). Today, vegetation dominated by Amaranthaceae is typically associated with desert or steppe-desert landscapes and is recorded in Iraq and Saudi Arabia (El-Moslimany, 1990), Armenia (Robles et al., 2022), China (e.g. Xu et al., 2009; Zhao and Herzschuh, 2009; Wei et al., 2011; Zheng et al., 2014; Wei and Zhao, 2016) and Mongolia (Ma et al., 2008; Zheng et al., 2014). *Ephedra* is a drought-tolerant shrub typical of arid and semi-arid regions (Herzschuh et al., 2004; Zheng et al., 2014). The *Ephedra distachya*-type is particularly associated with semi-desert conditions, especially in mountainous environments (Herzschuh et al., 2004; Zhao and Herzschuh, 2009). The dominance of Amaranthaceae, along with the consistent presence of *Ephedra distachya*-type suggests that PAZ 2 reflects drier conditions than the receding interval during the Early Pliocene. As previously noted, the arboreal taxa of *Quercus pubescens*-type and *Pinus* mediterranean-type are best interpreted as regional signals. Their relative stable presence in PAZ 2 does not contradict the inference of increasing aridity because they likely represent pollen input from surrounding upland areas rather than local woodland vegetation.

In PAZ 3 (Fig. 4A), the vegetation continues to reflect steppe conditions, dominated by Poaceae, Amaranthaceae, and *Artemisia.* A slight increase in arboreal pollen taxa is observed, primarily due to the rising

percentages of *Pinus* mediterranean-type and *Cedrus*. This trend is reflected in the PCA results, where samples from this zone show higher values on Axis 1 (Fig. 5), indicating a shift toward a greater arboreal component. During this interval, Poaceae and Amaranthaceae contribute similarly to the pollen signal. Although Poaceae is typically under-represented in pollen assemblages, often only accounting for a small fraction of the actual vegetation cover, it still constitutes around a quarter of the vegetation in Central Asia steppes (Ge et al., 2017). However, in the Caucasus, several studies have shown a stronger correspondence between Poaceae pollen and the actual vegetation cover (Connor et al., 2004; Robles et al., 2022). In contrast, Amaranthaceae pollen tends to be over-represented due to its high pollen production and long distance transport capacity (Li et al., 2005; Zheng et al., 2008). Given this differential representation, the steppe vegetation surrounding Burdur Basin during PAZ 3, was likely dominated by Poaceae. Modern analogues of Poaceae-dominated steppe vegetation are found in Georgia (Connor et al., 2004), Armenia (Robles et al., 2022), Iran (Djamali et al., 2009) and China (Zhao et al., 2009). This vegetation type is often occurs at high elevations, such as in Armenia, where Poaceae pollen dominates the signal from 1900 m and can account for up to 30% of the pollen record (Robles et al., 2022). As in previous zones, the arboreal taxa *Quercus pubescens*-type, *Pinus* mediterranean-type and *Cedrus* are interpreted as indicators of regional vegetation, with *Cedrus* likely originating from higher elevations. The concurrent increase in Poaceae and arboreal pollen suggests a phase of relatively wetter climatic conditions during PAZ 3.

During PAZ 4 (Fig. 4A), steppe vegetation remains dominate, composed primarily of Amaranthaceae, *Artemisia* and Poaceae, while arboreal pollen decreases sharply. This decline is reflected in the PCA results, with samples showing negative values on both Axis 1 and Axis 2 (Fig. 5), consistent with a landscape dominated by herbaceous steppic taxa. Amaranthaceae exceeds 50% of the pollen sum in this interval, suggesting a pronounced shift towards drier conditions relative to earlier phases.

In PAZ 5, marking the final phase of the Early Pliocene, steppe vegetation continues to include Poaceae, Amaranthaceae, and *Artemisia* (Fig. 4A). However, a notable increase in arboreal pollen is observed, including both deciduous taxa (*Quercus pubescens*-type, *Zelkova, Fraxinus*) and coniferous taxa (*Pinus* mediterranean-type*, P. sylvestris, Juniperus, Abies*). This shift is reflected by positive values on the PCA Axis 2 (Fig. 5), indicating an expansion of mesophilous arboreal vegetation. This combined increase in Poaceae and arboreal pollen taxa suggests more humid conditions compared to the receding period.

The Late Pliocene (Piacenzian, PAZ 6-7) is again characterized by steppe vegetation dominated by Amaranthaceae, Poaceae, and *Artemisia*, with a marked decline in arboreal pollen taxa (Fig. 4A; PAZ 6). PCA Axis 1 values for this zone are predominately negative, indicating increasingly open vegetation (Fig. 5). The strong dominance of Amaranthaceae (>50%) and reduced arboreal presence point to drier conditions, similar to those observed at the end of the Early Pliocene (PAZ 4).

In PAZ 7, the final zone in the sequence, steppe vegetation remains prominent (Poaceae, Amaranthaceae and *Artemisia),* but arboreal pollen increase once again, particularly from *Pinus* mediterranean-type*, P. sylvestris, Quercus pubescens*-type, and *Cedrus*. This shift is reflected in rising PCA Axis 1 values (Fig. 5), indicating a renewed development of arboreal vegetation, especially conifers. The percentage of Poaceae pollen exceeds 30%, suggesting steppe vegetation dominated by grasses. The co-occurrence of high Poaceae and increased arboreal pollen is indicative of more humid conditions during this interval.

In summary, the vegetation of Southwestern Anatolia during the Early-Late Pliocene transition is dominated by steppe vegetation, with periodic expansions of arboreal taxa under more humid conditions. This

pattern is comparable to that documented for the Pleistocene at Acıgöl Basin, where *Pinus* was more prominent during certain intervals (Andrieu-Ponel et al., 2021).

Vegetation changes around the Mediterranean Basin

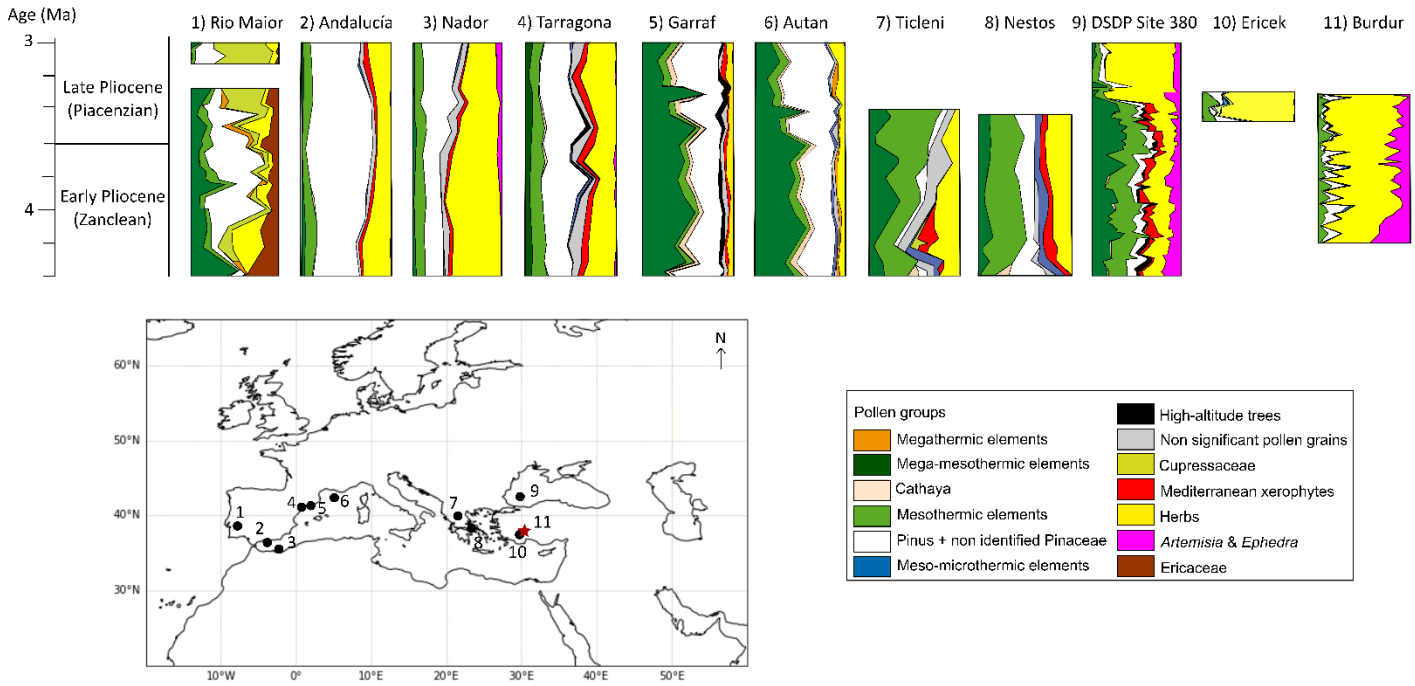

Figure 8: Vegetation changes around the Mediterranean Basin for the Early-Late Pliocene transition for selected palynological studies: 1) Rio Maior F16 (Diniz, 1984), 2) Andalucía G1 (Suc et al., 1995), 3) Nador (Feddi et al., 2011), 4) Tarragona E2 (Bessais and Cravatte, 1988), 5) Garraf 1 (Suc and Cravatte, 1982), 6) Autan 1 (Cravatte and Suc, 1981), 7) Ticleni 1 (Jiménez-Moreno et al., 2007), 8) Nestos 2 (Jiménez-Moreno et al., 2007), 9) DSDP site 380 (Popescu, 2006), 10) Ericek (Jiménez-Moreno et al., 2015) and 11) Burdur (this study) presented in percentages. The description of ecological classification of pollen taxa is presented in Supplementary Table S4.

Pollen records documenting the Early-Late Pliocene transition are primarily concentrated in the Western Mediterranean Basin (Fig. 8; e.g. Jiménez-Moreno et al., 2010; Suc et al., 2018) and the Balkans (Jiménez-Moreno et al., 2007), whereas continuous records for the Central Mediterranean are scarce (Combourieu-Nebout et al., 2015). In the Eastern Mediterranean, only a few sites span this interval, including the Black Sea (DSDP Site 180; Popescu, 2006) and Ericek in Southwestern Türkiye (Jiménez-Moreno et al., 2015). While other pollen records for Anatolia exist, their limited temporal resolution and imprecise chronologies preclude their inclusion in our comparison (Yavuz Işık et al., 2011; Alçiçek and Jiménez-Moreno, 2013; Kayseri-Özer et al., 2017; Tuncer et al., 2023; Tagliasacchi et al., 2024a).

During the latter part of the Early Pliocene (Zanclean period, 4–3.6 Ma), contrasting vegetation patterns are observed across the Mediterranean Basin (Fig. 8). Southern sites (Andalucía, Nador, Tarragona, Burdur) record predominantly open vegetation, while northern sites (Autan, Garraf, Nestos, Ticleni, DSDP Site 380) are dominated by deciduous forest taxa (Cravatte and Suc, 1981; Suc and Cravatte, 1982; Bessais and Cravatte, 1988; Suc et al., 1995; Jiménez-Moreno et al., 2007; Popescu et al., 2010; Feddi et al., 2011). The latitudinal boundary between these vegetation zones varies by longitude and is influenced by local geographical settings, as illustrated by the contrast between Tarragona and nearby Garraf. On the Atlantic side of the Iberian Peninsula, Rio Maior

site (Diniz, 1984) is distinct for its dominance of mega-mesothermic trees taxa and Ericaceae, the latter being a characteristic of modern Atlantic coast vegetation. In Southern Iberian, the Andalucía and Nador sites exhibit herb-rich assemblages and *Pinus* reflecting sub-desertic vegetation similar to that seen today parts of the Southwestern Mediterranean (Suc et al., 1995; Feddi et al., 2011). Northwestern Spain, yields mixed results, with Tarragona showing open herbaceous pollen assemblages and *Pinus* (Bessais and Cravatte, 1988), while Garraf in Northwestern Spain (Suc and Cravatte, 1982) and Autan in the South of France (Cravatte and Suc, 1981) are characterized by mega-mesothermic trees. In the Balkans, Nestos and Ticleni also contain abundant mesothermic and megathermic taxa (Jiménez-Moreno et al., 2007 and references therein). Further east, the Black Sea record (DSDP Site 380) reveals extensive mega-mesothermic and mesothermic elements, such as Cupressaceae and *Cathaya* (Popescu et al., 2010), suggesting relatively humid, temperate environments along coastal plains. In contrast, the Burdur record from Southwestern Türkiye documents open steppe vegetation dominated by Amaranthaceae, *Artemisia* and Poaceae, with minimal arboreal pollen and no relict taxa. Although the presence of *Artemisia* steppe in Anatolia during the Early Pliocene has been previously suggested (Popescu, 2006; Suc et al., 2018), the Burdur sequence shows that steppe composition varied through time, with different periods dominated by *Artemisia*, Amaranthaceae, or Poaceae. Elsewhere in Anatolia, the Çankırı-Çorum sequence from the central region indicates similarly open vegetation dominated by Poaceae, Amaranthaceae and Urticaceae; however, the sequence is poorly dated and may represent a period earlier than 4 Ma (Kayseri-Özer et al., 2017). Another sequence from Southwestern Anatolia (Şarkikaraağaç) is characterized by a dominance of Pinaceae and Amaranthaceae (Tuncer et al., 2023). The precise Pliocene age of this record, however, remains uncertain, and it is based on a limited number of samples (n = 7). Nevertheless, the presence of *Cathaya* may suggest an attribution to the Early Pliocene. In Central Asia, on the Tibetan Plateau, Pliocene vegetation was also dominated by semi-desert and desert elements, such as Amaranthaceae, *Artemisia*, Poaceae and Cyperaceae reflecting similar arid or semi-arid conditions (Koutsodendris et al., 2019; Schwarz et al., 2023).

At the transition between the Early and Late Pliocene (Piacenzian, 3.6–3.4 Ma), substantial vegetation changes are recorded around the Mediterranean Basin, notably marked by the expansion of deciduous trees (Fig. 8). However, a distinct west-east contrast is observed: western regions (Rio Maior, Andalucía, Nador, Tarragona, Garraf) show a marked dominance of *Pinus*, while eastern regions (DSDP Site 180, Ericek, Burdur) are more characterized by open herbaceous-dominated vegetation (Cravatte and Suc, 1981; Suc and Cravatte, 1982; Bessais and Cravatte, 1988; Diniz, 1984; Suc et al., 1995; Popescu et al., 2010; Feddi et al., 2011; Jiménez-Moreno et al., 2015). In the Western Mediterranean, sites such as Rio Maior, Garraf and Autan record a significant decline in mega-mesothermic elements, accompanied by a notable increase of *Pinus* (Suc and Cravatte, 1982; Cravatte and Suc, 1981; Diniz, 1984). In the south of Spain (Andalucía), and Northern Morocco (Nador), herbaceous taxa remain abundant, but open formations shift toward steppe vegetation dominated by *Artemisia* and *Ephedra*. The Nador record also shows a pronounced increase in *Pinus*, while high altitude conifers such as *Cedrus*, *Tsuga* or *Cathaya* appear alongside Mediterranean xerophytes including *Olea*, *Quercus* type *ilex-coccifera* in Andalucía (Suc et al., 1995; Feddi et al., 2011). In contrast, Eastern Mediterranean records show a general decline in arboreal pollen taxa during this period. The decline is abrupt in the Black Sea record (DSDP Site 380; Popescu, 2006) and more gradual in Southwestern Anatolia, including Burdur (this study). Herbaceous taxa dominate these sequences, indicating the persistence of open vegetation. At Ericek in the Çameli Basin of Southwestern Anatolia, open steppe vegetation with a high proportion of Poaceae is observed, and relict taxa are largely absent; however, the record is

based on a limited number of pollen samples (n=7, Jiménez-Moreno et al., 2015). Moreover, in the Karacasu Basin of Southwestern Anatolia, open steppe vegetation dominated by Poaceae is also observed, however, the record is based on a limited number of pollen samples, and its precise Pliocene age remains uncertain (n=5, Alçiçek and Jiménez-Moreno, 2013). Similarly, in Burdur, vegetation remains predominately steppic, with alternating dominance of Poaceae and Amaranthaceae, and no relict taxa detected. In contrast, the Karahallı site (Southwestern Anatolia) records the presence of Pinaceae, *Cathaya*, Cupressaceae, and Asteraceae dated to the Early–Late Pliocene transition and possibly reflecting regional diversity (Tagliasacchi et al., 2024b). Yet this sequence is restricted to six samples and exhibits limited taxonomic diversity. Another sequence from central Anatolia (Akçaköy) also indicates a dominance of Pinaceae and Asteraceae (Yavuz Işık et al., 2011), but its precise Pliocene age remains uncertain, and it is based on only five samples. Beyond the Mediterranean, the Central Asian records (e.g., Koutsodendris et al., 2019; Schwarz et al., 2023), show persistent desert and semi-desert vegetation dominated by Amaranthaceae, *Artemisia*, Poaceae, Cyperaceae, and *Ephedra*. Since the Late Pliocene, these records exhibit an increase of Amaranthaceae and an alternation between desert vegetation (dominated by Amaranthaceae), and steppe vegetation (dominated by *Artemisia,* with increasing Poaceae. A comparable alternation is evident at Burdur, where phases of Amaranthaceae-dominated and Poaceae-dominated steppe alternate through time. The observed differences between Central Asia and Southwestern Anatolia, particularly the dominance of Poaceae at Burdur versus *Artemisia* in Central Asia, likely reflect regional contrasts in precipitation regimes and climate seasonality.

5.3 Climate changes around the Mediterranean Basin during the Early-Late Pliocene transition

Climate changes in southwestern Anatolia

Pollen-inferred climate changes have been reconstructed for the first time for a pre-Quaternary period using a multi-method approach. The Climatic Amplitude Method (CAM) is typically applied to Neogene sequences, where fossil pollen assemblage lack modern analogues (Fauquette et al., 1998a, b). However, the Burdur record, characterized by steppe vegetation and lacking relict taxa (Fig. 4A), permits the application of other commonly used techniques for Quaternary climate reconstruction, (MAT, WA-PLS, etc.). The climate reconstructions from Burdur show broadly consistent trends across most methods, with the exception of CAM, particularly during the Late Pliocene (Fig. 7). As frequently observed in open-vegetation environments (Fauquette et al., 1999), the climatic intervals reconstructed using CAM are wider (Supplementary Table S3), owing to the absence of relict taxa and the broader ecological range of taxa like Poaceae, which limits the precision of climate estimates. The RandomForest (RF) method tends to overestimate seasonal precipitation values compared to other methods (Fig. 7), likely due to the relative contribution of taxa with the highest percentages that are ecologically limited and poor pollen producers in the study site (Salonen et al., 2019). In contrast, the most statistically robust reconstructions across all climatic parameters are obtained using the BRT and MAT methods, which yield the highest R^2 and lowest RMSE values (Supplementary Table S1). For MAT, spatial autocorrelation is low (Moran's $I<0.19$, p-value<0.01) and for BRT, the boosting algorithm significantly enhances model performance, making it particularly effective for microfossil based reconstructions (Salonen et al., 2019; Chevalier et al., 2020). Based on these performance metrics and to facilitate comparison with prior Mediterranean pollen-inferred climate reconstructions (Fauquette et al., 2007), results from MAT, BRT, and CAM are retained for discussion.

The climate reconstructions from Burdur pollen assemblages indicate Mediterranean climate conditions, with hot, dry summers and cool winters throughout the Pliocene (Fig. 7). The reconstructions suggest a climatic optimum in terms of precipitation and temperature (PAZ 1 and 2) followed by an alternation between cool, wet phases (PAZ 3, 5, and 7) and warm, dry intervals (PAZ 4 and 6). Notably, the amplitude of climatic oscillations reconstructed with MAT appear larger than expected for this period. Previous studies (Suc, 1984; Suc et al., 2018), have proposed that the onset of a Mediterranean-type seasonal regime climate, with summer drought and cool, wet winters, occurred during the Pliocene. At Burdur, a similar pattern emerges, with Mediterranean conditions particularly evident during summer. However, winter precipitation appears lower than today, suggesting overall more arid winter conditions compared to the modern Mediterranean climate.

Climate changes around the Mediterranean Basin

Pollen-inferred climate reconstructions from the Mediterranean Basin, particularly in its western region, have primarily used CAM (Fig. 9; Fauquette et al., 1998a, 1999, 2007; Jiménez-Moreno et al., 2010; Feddi et al., 2011). During the final part of the Early Pliocene (Zanclean period, 4–3.6 Ma), CAM-based reconstructions indicate warmer-than-present conditions at sites including Rio Maior, Andalucía, Nador, Tarragona, and Garraf (Fauquette et al., 1998a, 1999, 2007). These results are consistent with the temperature trends reconstructed at Burdur using CAM, while other methods (except for MTWA with MAT and WA-PLS) do not replicate this warming signal (Fig. 8). Other proxies also support a global climatic context warmer than today for this period (Fig. 9). The LR04 benthic oxygen isotope stack (Lisiecki and Raymo, 2005) and the Global Reference benthic foraminifer oxygen isotope dataset (Westerhold et al., 2020) show lower $\delta^{18}O$ values than today, reflecting elevated global temperatures and reduced ice volume prior to the intensification of the Northern Hemisphere glaciation (Maslin et al., 1998). Around the Mediterranean Basin (Fig. 9), sea surface temperature (SST) reconstructions based on alkenones from Cyprus similarly indicate warmer-than-modern conditions during the Zanclean (Athanasiou et al., 2017), although a transient cooling event at ~3.91 Ma is recorded and corresponds to the global MIS Gi16 (Athanasiou et al., 2017). Further temperature reconstructions from the Teruel (Spain), based on lacustrine $\delta^{18}O_c$ (Ezquerro et al., 2022), and on planktonic $\delta^{18}O$ records from Cyprus and Italy (Medstack; Wang et al., 2010; Colleoni et al., 2012) also indicate generally warm climatic conditions. The temperature reconstructions for Burdur using CAM are consistent with these regional and global datasets. Additionally, MTWA values reconstructed using MAT, agree with alkenone-based SST reconstructions from the Eastern Mediterranean (Athanasiou et al., 2017), likely reflecting summer temperatures.

In terms of precipitation (Fig. 9), reconstructions of the Early Pliocene suggest values close to modern conditions in Southern Iberia (Andalucía, Nador and Tarragona), while more humid conditions are recorded for Northern Iberia (Garraf) (Fauquette et al., 1998a, 1999, 2007). Similarly, in the Eastern Mediterranean, pollen-inferred climate reconstructions at Burdur indicate precipitation levels roughly equivalent to present (Fig.7). As previously highlighted by Fauquette et al. (2007) and Jiménez-Moreno (2010), these reconstructions suggest a persistent north-south precipitation gradient, with wetter conditions in the Northern Mediterranean. However, many available records suffer from low temporal resolution and limited spatial coverage, particularly in the Eastern Mediterranean. High-resolution reconstructions remain critically needed to clarify regional variability and climate dynamics during this period. Climatic variability in the Mediterranean region during this Zanclean was modulated

by orbital forcing, particularly the 23-ka precession cycle, and by the changes in African monsoon intensity (Colleoni et al., 2012; Athanasiou et al., 2017), which likely influenced precipitation across the basin.

During the Late Pliocene (Piacenzian period, 3.6–3 Ma; Fig. 9), pollen-inferred climate reconstructions indicate warmer-than-present temperatures in the Western Mediterranean (Rio Maior, Andalucía, Nador, Tarragona, and Garraf) by Fauquette et al. (1998, 1999, 2007). Similar results are obtained for Burdur using CAM, whereas other methods suggest lower values than present (Fig. 7). Global oxygen isotope records (Fig. 9), including the LR04 benthic stack (Lisiecki and Raymo, 2005) and the Global Reference benthic foraminifer dataset (Westerhold et al., 2020), also support a warmer-than-modern climate during this period. In the Mediterranean Basin (Fig. 9), regional $\delta^{18}O$ stack (Medstack; Wang et al., 2010; Colleoni et al., 2012) and SST reconstructions based on alkenones, showing values approximately 4 °C higher than today, from Cyprus (Athanasiou et al., 2017) and Italy (Herbert et al., 2015; Plancq et al., 2015) confirm these warmer conditions. At Burdur, the transition between Early and Late Pliocene is marked by a decrease in reconstructed temperatures using the BRT and MAT methods, but not CAM. This cooling trend is also reflected in LR04 benthic stack (Lisiecki and Raymo, 2005) and the Global Reference benthic foraminifer Dataset (Westerhold et al., 2020), as well as the Medstack (Wang et al., 2010; Colleoni et al., 2012). SST data from Cyprus shows a similar decline, with cooling events identified at 3.58 Ma and 3.34–3.31 Ma, corresponding to MIS MG12 and MIS M2 (Plancq et al., 2015; Athanasiou et al., 2017). A significant decrease in temperature is also evident at the Teruel site in Spain, based on lacustrine $\delta^{18}O_c$ values from 3.6 to 3 Ma (Ezquerro et al., 2022). However, in the Western Mediterranean, pollen-inferred temperature trends across the Early–Late Pliocene transition are less evident, likely due to the limited temporal resolution of available records. During the Late Pliocene, the Mediterranean climate variability continued to be paced by the 23-ka precession cycle, and the intensified African monsoonal activity (Herbert et al., 2015; Athanasiou et al., 2017). Obliquity-driven rhythms became influential on SSTs from 2.8 Ma and dominated after 2.51 Ma (Herbert et al., 2015).

In terms of precipitation (Fig. 9), the Western Mediterranean shows a general increase at sites such as Rio Maior, and Nador, (Fauquette et al., 1998a, 1999, 2007), while sites like Andalucía Tarragona and Garraf record few changes during the Late Pliocene. Again, low-resolution sampling limits interpretation, and more detailed records are needed to fully understand the changes during this period. In the Eastern Mediterranean, Burdur also shows precipitation values close to today, except for winter precipitation, which appears lower (Fig. 7). Aridity estimates at Teruel (Spain), based on lacustrine $\delta^{18}O_c$, suggest increased humidity, particularly between 3.6 and 3 Ma (Ezquerro et al., 2022). In Cyprus and Italy, planktonic $\delta^{18}O$ records show a more progressive decline in precipitation during the Late Pliocene (Medstack; Wang et al., 2010; Colleoni et al., 2012). In Central Asia, dry conditions are inferred from 3.8 Ma, likely linked to a weakening of the East Asian Monsoon (Schwarz et al., 2023). Thus, the Late Pliocene appears to be marked by more humid conditions in the Western Mediterranean, while more arid conditions prevailed in Southwestern Türkiye and Central Asia. A weak Atlantic Meridional Overturning Circulation (AMOC) between 3.8 to 3 Ma, may have contributed to cooler and wetter conditions primarily in the Northwestern Mediterranean (Karas et al., 2017; Ezquerro et al., 2022).

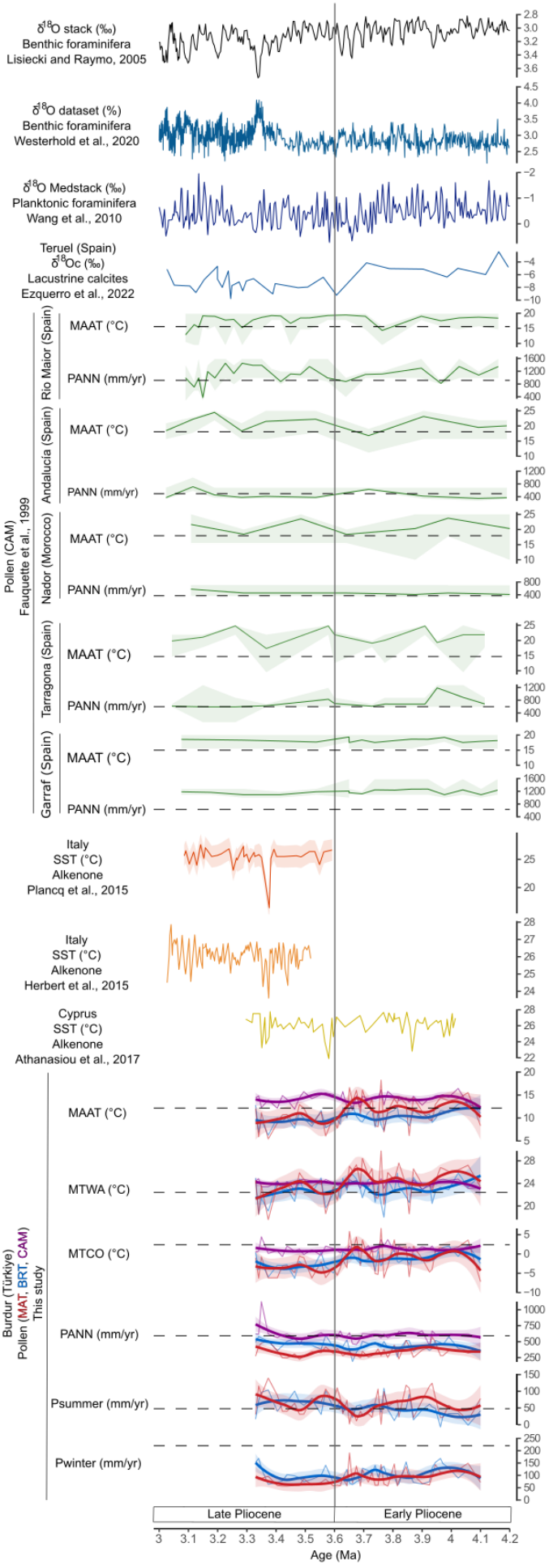
δ18O stack (‰)
Benthic foraminifera
Lisiecki and Raymo, 2005
δ18O dataset (%)
Benthic foraminifera
Westerhold et al., 2020
δ18O Medstack (‰)
Planktonic foraminifera
Wang et al., 2010
Teruel (Spain)
δ18Oc (‰)
Lacustrine calcites
Ezquerro et al., 2022
Pollen (CAM)
Fauquette et al., 1999
Rio Maior (Spain)
MAAT (°C)
PANN (mm/yr)
Andalucia (Spain)
MAAT (°C)
PANN (mm/yr)
Nador (Morocco)
MAAT (°C)
PANN (mm/yr)
Tarragona (Spain)
MAAT (°C)
PANN (mm/yr)
Garraf (Spain)
MAAT (°C)
PANN (mm/yr)
Italy
SST (°C)
Alkenone
Plancq et al., 2015
Italy
SST (°C)
Alkenone
Herbert et al., 2015
Cyprus
SST (°C)
Alkenone
Athanasiou et al., 2017
Burdur (Türkiye)
Pollen (MAT, BRT, CAM)
This study
MAAT (°C)
MTWA (°C)
MTCO (°C)
PANN (mm/yr)
Psummer (mm/yr)
Pwinter (mm/yr)
Late Pliocene
Early Pliocene
Age (Ma)

Figure 9. Climate reconstructions from global and Mediterranean records for the Early-Late Pliocene transition (4.2–3.0 Ma), arranged west to east. Global records include the $\delta^{18}O$ stack (Lisiecki and Raymo, 2005) and the $\delta^{18}O$ dataset (Westerhold et al., 2020). Mediterranean records include the $\delta^{18}O$ Medstack (Wang et al., 2010), $\delta^{18}Oc$ from Teruel (Ezquerro et al., 2022), pollen-based climate reconstructions from Rio Maior, Andalucía, Nador, Tarragona, and Garraf using the Climatic Amplitude Method (CAM; Fauquette et al., 1999), alkenone-based sea surface temperatures (SSTs) from Italy (Herbert et al., 2015; Plancq et al., 2015) and Cyprus (Athanasiou et al., 2017), pollen-inferred climate reconstructions from Burdur (this study), using CAM, Modern Analogue Technique (MAT), and Boosted Regression Trees (BRT). Black dashed lines correspond to modern climate values. MAAT: mean annual temperature. MTWA: mean temperature of the warmest month. MTCO: mean temperature of the coldest month. PANN: mean annual precipitation. Psummer: summer precipitation. Pwinter: winter precipitation.

Late Pliocene model–data comparison for the Mediterranean Basin

The Pliocene Model Intercomparison Project Phase 2 (PlioMIP2) includes results from 13 coupled atmosphere-ocean global climate models (GCMs) simulating climate during the mid-Pliocene Warm Period (mPWP; 3.264–3.025 Ma), using boundary conditions based on the PRISM4 data set (Feng et al., 2022). These conditions incorporate land-sea distribution, topography, bathymetry, vegetation, soils, lakes, and land ice cover, with atmospheric pCO_2 set at 400 ppmv. A compilation of 62 global proxy records, including sedimentological indicators, palynological, floral or faunal, offshore marine records, and stable isotope analyses of organic and inorganic materials were assembled by Feng et al. (2022). Each record was classified as indicating wetter, drier, or unchanged conditions compared to late Quaternary or modern climates. In the present study, we focus on the Mediterranean Basin, including 18 proxy records from Feng et al. (2022) and the Burdur record (this study) as an additional point (Fig. 10). Despite the Burdur sequence terminating at 3.33 Ma, slightly older than the mPWP interval, it is included due to the scarcity of high-resolution records and limited regional model coverage.

PlioMIP2 simulations for 3.264 and 3.025 Ma indicate warmer temperatures 2.6-4.8 °C higher than pre-industrial levels (Haywood et al., 2020), in line with proxy-based reconstructions (Fig. 9, 10). Precipitation simulations show a latitudinally structured pattern: wetter conditions in Northern Europe and drier or unchanged conditions across Southern Europe and the Mediterranean (Fig. 10). For Southern Spain, Southern Italy, Greece, and Türkiye, simulations suggest conditions comparable to or slightly more arid than present (Haywood et al., 2020; Feng et al., 2022). Proxy-based climate reconstructions are broadly consistent with model simulations in Southern Spain and Southwestern Türkiye. However, in Western and Northern Spain, Southern France, and part of Italy, proxies indicate wetter conditions than those simulated. In the Eastern Mediterranean, the spatial variability is more complex. Proxy reconstructions suggest wetter conditions in Central Anatolia, the Southeastern Mediterranean, and the Eastern Caucasus (sites 14‑16, 19; Horowitz, 1989; Gürel and Yıldız, 2007; Salzmann et al., 2008; Vaks et al., 2013), whereas simulations predict drier conditions. Only two sites, Burdur (this study) and the Kerch Peninsula (site 17; Salzmann et al., 2008), show agreement between proxy and model, both indicating drier or near-modern conditions.

Several factors may explain the differences between proxy records and the PlioMIP2 simulations. Firstly, many proxy datasets represent average or time-integrated climate signals due to coarse temporal resolution and dating uncertainties, while models simulate a narrow time window using fixed orbital parameters (Haywood et al., 2020; Feng et al., 2022). Secondly, regional topography and land-sea contrasts, which are critical to local climate dynamics, may be insufficiently resolved in GCMs. Third, vegetation and ice sheet feedbacks, important long-term components of Earth system, are not fully incorporated into many model configurations (Feng et al., 2022). Additionally, while model ensembles agree over some regions (e.g., Sahel and East Asia), they show divergent spatial signals elsewhere, especially in mid-latitudes (Feng et al., 2022).

Despite these limitations, both proxy data and model simulations, support the hypothesis of a weakened AMOC during 3.8 and 3 Ma, resulting in cooler and wetter conditions, particularly in the Northwestern Mediterranean. However, PlioMIP2 simulations suggest this wetter zone is located farther north on the Iberian Peninsula compared to proxy evidence. In the Eastern Mediterranean, strong regional variability inferred from proxy data is not captured by model outputs. Nevertheless, the Burdur site shows drier or near-modern conditions during the mPWP, aligning with model simulations and contributing value regional insight to the mid-Pliocene climatic mosaic.

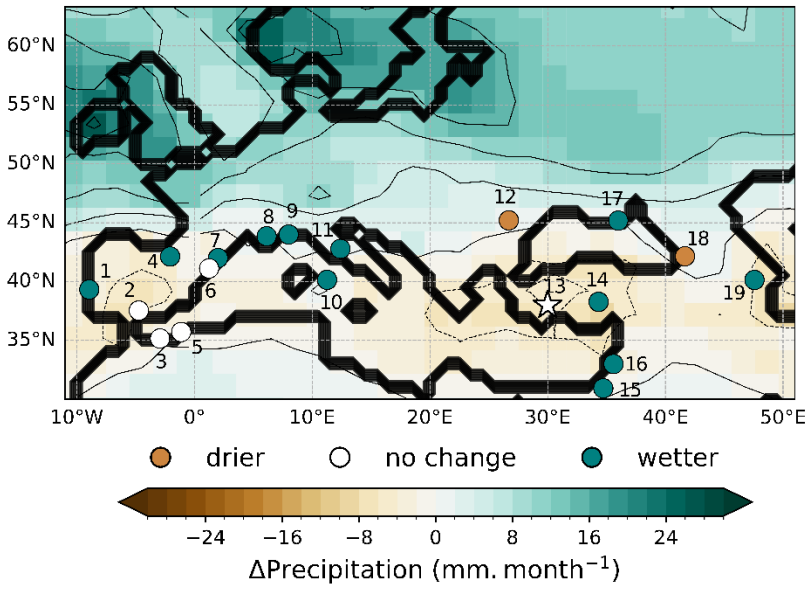

Figure 10: Model-Data comparison from 3.264 to 3.025 Ma. Precipitation anomalies and comparison between PlioMIP2 and selected data around the Mediterranean Basin: 1) Rio Maior F16 (Fauquette et al., 1999), 2) Andalucía G1 (Fauquette et al., 1999), 3) Nador (Fauquette et al., 1999), 4) Villarroya (Muñoz et al., 2002; Anadón et al., 2008) (Munoz et al., 2002; Anadon et al., 2008), 5) Habibas 1 (Fauquette et al., 1999), 6) Tarragona E2 (Fauquette et al., 1999), 7) Garraf (Fauquette et al., 2007), 8) Puimoisson (Blavoux et al., 1999), 9) St Isidore (Fauquette et al., 2007), 10) ODP 653 (Bertoldi et al., 1989), 11) Tiberino Basin (Basilici, 1997), 12) Dacian Basin (Van Baak et al., 2015), 13) Burdur (this study), 14) Ihlara-Selime (Gürel and Yıldız, 2007), 15) Ashalim Cave (Vaks et al., 2013), 16) Hula Basin (Horowitz, 1989), 17) Kerch Peninsula (Salzmann et al., 2008), 18) Colchis (Shatilova, 1986), 19) Azerbaijan (Salzmann et al., 2008). Data originating from Feng et al., 2022.

6. Conclusion

Based on the new high-resolution pollen sequence from Burdur sequence, this study provides valuable insights into the environmental and climatic changes during the poorly documented Early–Late Pliocene transition in the Eastern Mediterranean and more particularly in Southwestern Anatolia. The Burdur record reveals an open vegetation landscape, alternating between steppe grasslands with deciduous *Quercus* and steppes dominated by Amaranthaceae. The lacustrine ecosystem was characterized by semi-aquatic vegetation and freshwater algae, reflecting shifts between oligotrophic and eutrophic conditions. Although large Poaceae pollen grains are present, their percentages remain relatively low compared to those from Lake Acıgöl (a younger record), and their morphological characteristics do not permit a clear distinction between wild and domesticated types.

Pollen-based climate reconstructions suggest a climatic optimum in terms of precipitation and temperature prior to the Early–Late Pliocene transition, followed by alternating phases of relatively cool, wet

conditions and warm, dry conditions after the Early–Late Pliocene transition. At a Mediterranean scale, the Early Pliocene shows contrasting north-south pattern: southern regions were characterized by open steppe-like vegetation, while northern and central areas were dominated by deciduous forests. Multiple proxy records point to warmer-than-modern conditions during this period, with a noticeable north-south precipitation gradient, favoring wetter wetter conditions in the Northern Mediterranean.

The Late Pliocene marks a shift: while deciduous trees expand in many regions, vegetation dynamics diverged across the basin. Western Mediterranean sites became dominated by *Pinus*, while eastern records, including Burdur, continued to reflect open vegetation and steppe environments. During this time, cooler conditions prevailed, with more humid climates in the Western Mediterranean contrasting with more arid conditions in Southwestern Türkiye and Central Asia. A weakened AMOC between 3.8 to 3 Ma may have contributed to cooler and wetter conditions in the Northwestern Mediterranean.

PlioMIP2 simulations for the mid-Pliocene Warm Period (3.264–3.025 Ma) indicate a generally warmer climate and a latitudinal precipitation gradient, wetter in Northern Europe, drier in the southern. While these simulations align with some proxy records, they fail to fully capture the spatial complexity of the Eastern Mediterranean climate, where the Burdur record supports drier or near-modern conditions, in contrast to wetter conditions inferred from other nearby regions.

This study underscores the spatial heterogeneity and complexity of vegetation and climate responses across the Mediterranean during the Pliocene. It highlights the value of high-resolution, regionally focused records for refining global and regional climate models. Understanding the mechanisms and impacts of Pliocene climate variability offers critical insights into the potential trajectories and uneven regional consequences of current and future climate change. Future efforts should focus on increasing the number of well-dated, high-resolution records in the Eastern Mediterranean in order to better constrain regional environmental variability.

Author contribution

MR: Laboratory work (pollen, NPPs), Formal analysis (climate reconstruction), Writing draft manuscript. VA: Conceptualization, Core sampling, Review & editing, Funding acquisition. PR: Laboratory work (paleomagnetism), Review & editing. SF: Formal analysis (climate reconstruction for CAM method), Review & editing. OPe: Review & editing. FD: Laboratory work (paleomagnetism), Review & editing. OPa: Core sampling. EC: Laboratory work (pollen extraction). BG: Review & editing. MCA: Laboratory work (magnetic susceptibility), Review & editing.

Declaration of competing interest

At least one of the (co-)authors (O. Peyron) is a member of the editorial board of Climate of the Past but the authors declare that they have no known competing financial interests or personal relationships that could have appeared to influence the work reported in this paper.

Funding

This study was financially supported by ANR FOOD-RE (ANR-21-CE03-0019) V. Andrieu leader 1 April 2022 (https://www.cerege.fr/fr/sciences/terre-et-planetes/projets-terre-et-planete/anr-food-re). The geological fieldwork done my MCA was funded by the Scientific and Technological Research Council of Türkiye

(TÜBİTAK) under the research grant ÇAYDAG 105Y280. Conference funding was provided by the Association des Palynologues de Langue Française (APLF).

Acknowledgements

The studied core was collected as part of the Huntite Exploration Project in the Lake District, conducted by the Mineral Research and Exploration Directorate of Türkiye (MTA), under Project Number 2018-32-13-21. The authors would like to thank Gonzalo Jiménez-Moreno for providing access to the pollen data of Ericek. We also thank the editor and the two anonymous reviewers for their reading and constructive comments. This is an ISEM contribution n°2025-167.

References

Alçiçek, H. and Jiménez-Moreno, G.: Late Miocene to Plio-Pleistocene fluvio-lacustrine system in the Karacasu Basin (SW Anatolia, Turkey): Depositional, paleogeographic and paleoclimatic implications, Sedimentary Geology, 291, 62–83, https://doi.org/10.1016/j.sedgeo.2013.03.014, 2013.

Alçiçek, M. C., Mayda, S., and Titov, V. V.: Lower Pleistocene stratigraphy of the Burdur Basin of SW Anatolia, Comptes Rendus Palevol, 12, 1–11, https://doi.org/10.1016/j.crpv.2012.09.005, 2013a.

Alçiçek, M. C., Brogi, A., Capezzuoli, E., Liotta, D., and Meccheri, M.: Superimposed basin formation during Neogene–Quaternary extensional tectonics in SW-Anatolia (Turkey): Insights from the kinematics of the Dinar Fault Zone, Tectonophysics, 608, 713–727, https://doi.org/10.1016/j.tecto.2013.08.008, 2013b.

Alçiçek, M. C., Mayda, S., and Demirel, F. A.: Discussion on Neogene-Quaternary evolution of the Tefenni basin on the Fethiye-Burdur fault zone, SW Anatolia-Turkey, Journal of African Earth Sciences, 134, 794–799, https://doi.org/10.1016/j.jafrearsci.2016.07.024, 2017.

Alçiçek, M. C., Mayda, S., ten Veen, J. H., Boulton, S. J., Neubauer, T. A., Alçiçek, H., Tesakov, A. S., Saraç, G., Hakyemez, H. Y., Göktaş, F., Murray, A. M., Titov, V. V., Jiménez-Moreno, G., Büyükmeriç, Y., Wesselingh, F. P., Bouchal, J. M., Demirel, F. A., Kaya, T. T., Halaçlar, K., Bilgin, M., and van den Hoek Ostende, L. W.: Reconciling the stratigraphy and depositional history of the Lycian orogen-top basins, SW Anatolia, Palaeobio Palaeoenv, 99, 551–570, https://doi.org/10.1007/s12549-019-00394-3, 2019.

Anadón, P., Utrilla, R., Vázquez, A., Martín-Rubio, M., Rodriguez-Lázaro, J., and Robles, F.: Paleoenvironmental evolution of the Pliocene Villarroya Lake, northern Spain, from stable isotopes and trace-element geochemistry of ostracods and molluscs, J Paleolimnol, 39, 399–419, https://doi.org/10.1007/s10933-007-9121-2, 2008.

Andersen, S. T.: Identification of wild grass and cereal pollen, Danmarks Geologiske Undersøgelse Årbog, 69-92., 1979.

Andrieu, V. and Gambin, B.: An illustrated protocol for extracting palynomorphs from Early Pleistocene pollen-poor sediments using LST Fastfloat, Review of Palaeobotany and Palynology, 341, 105372, https://doi.org/10.1016/j.revpalbo.2025.105372, 2025.

Andrieu-Ponel, V., Rochette, P., Demory, F., Alçiçek, H., Boulbes, N., Bourlès, D., Helvacı, C., Lebatard, A.-E., Mayda, S., Michaud, H., Moigne, A.-M., Nomade, S., Perrin, M., Ponel, P., Rambeau, C., Vialet, A., Gambin, B., and Alçiçek, M. C.: Continuous presence of proto-cereals in Anatolia since 2.3 Ma, and their possible co-evolution with large herbivores and hominins, Sci Rep, 11, 8914, https://doi.org/10.1038/s41598-021-86423-8, 2021.

Athanasiou, M., Bouloubassi, I., Gogou, A., Klein, V., Dimiza, M. D., Parinos, C., Skampa, E., and Triantaphyllou, M. V.: Sea surface temperatures and environmental conditions during the "warm Pliocene" interval (~ 4.1–3.2 Ma) in the Eastern Mediterranean (Cyprus), Global and Planetary Change, 150, 46–57, https://doi.org/10.1016/j.gloplacha.2017.01.008, 2017.

Basilici, G.: Sedimentary facies in an extensional and deep-lacustrine depositional system: the Pliocene Tiberino Basin, Central Italy, Sedimentary Geology, 109, 73–94, https://doi.org/10.1016/S0037-0738(96)00056-5, 1997.

Bering, D.: The development of the Neogene and Quaternary intram ontane basins within the Pisidic lake d istrict in S. Anatolia, Newsletters on Stratigraphy, 27–32, https://doi.org/10.1127/nos/1/1971/27, 1971.

Bertini, A.: Pliocene to Pleistocene palynoflora and vegetation in Italy: State of the art, Quaternary International, 225, 5–24, https://doi.org/10.1016/j.quaint.2010.04.025, 2010.

Bertoldi, R., Rio, D., and Thunell, R.: Pliocene-pleistocene vegetational and climatic evolution of the south-central mediterranean, Palaeogeography, Palaeoclimatology, Palaeoecology, 72, 263–275, https://doi.org/10.1016/0031-0182(89)90146-6, 1989.

Bessais, E. and Cravatte, J.: Les écosystèmes végétaux Pliocènes de catalogne méridionale. Variations latitudinales dans le domaine nord-ouest méditerranéen, Geobios, 21, 49–63, https://doi.org/10.1016/S0016-6995(88)80031-7, 1988.

Beug, H.-J.: Leitfaden der Pollenbestimmung für Mitteleuropa und angrenzende Gebiete, Friedrich Pfeil, München, 542 pp., 2004.

Biltekin, D., Popescu, S.-M., Suc, J.-P., Quézel, P., Jiménez-Moreno, G., Yavuz, N., and Çağatay, M. N.: Anatolia: A long-time plant refuge area documented by pollen records over the last 23 million years, Review of Palaeobotany and Palynology, 215, 1–22, https://doi.org/10.1016/j.revpalbo.2014.12.004, 2015.

Blavoux, B., Dubar, M., and Daniel, M.: Indices isotopiques (13C et 18O) d'un important refroidissement du climat à la fin du Pliocène (formation lacustre de Puimoisson, Alpes-de-Haute-Provence, France), Comptes Rendus de l'Académie des Sciences - Series IIA - Earth and Planetary Science, 329, 183–188, https://doi.org/10.1016/S1251-8050(99)80233-X, 1999.

Bozkurt, E.: Origin of NE-trending basins in western Turkey, Geodinamica Acta, 16, 61–81, https://doi.org/10.1016/S0985-3111(03)00002-0, 2003.

ter Braak, C. J. F. and van Dam, H.: Inferring pH from diatoms: a comparison of old and new calibration methods, Hydrobiologia, 178, 209–223, https://doi.org/10.1007/BF00006028, 1989.

ter Braak, C. J. F. and Juggins, S.: Weighted averaging partial least squares regression (WA-PLS): an improved method for reconstructing environmental variables from species assemblages, Hydrologia, 269, 485–502, https://doi.org/10.1007/978-94-017-3622-0_49, 1993.

Brewer, S., Guiot, J., Sánchez-Goñi, M. F., and Klotz, S.: The climate in Europe during the Eemian: a multi-method approach using pollen data, Quaternary Science Reviews, 27, 2303–2315, https://doi.org/10.1016/j.quascirev.2008.08.029, 2008.

Brierley, C. M., Fedorov, A. V., Liu, Z., Herbert, T. D., Lawrence, K. T., and LaRiviere, J. P.: Greatly Expanded Tropical Warm Pool and Weakened Hadley Circulation in the Early Pliocene, Science, 323, 1714–1718, https://doi.org/10.1126/science.1167625, 2009.

Brown, T. A., Jones, M. K., Powell, W., and Allaby, R. G.: The complex origins of domesticated crops in the Fertile Crescent, Trends in Ecology & Evolution, 24, 103–109, https://doi.org/10.1016/j.tree.2008.09.008, 2009.

Charton, L., Combourieu-Nebout, N., Bertini, A., Lebreton, V., Peyron, O., Robles, M., Sassoon, D., and Moncel, M.-H.: Vegetation and climate changes during the Middle to Upper Palaeolithic transition in the southwestern Mediterranean: What happened to the last Neanderthals during Heinrich stadial 4?, Quaternary Science Reviews, 359, 109345, https://doi.org/10.1016/j.quascirev.2025.109345, 2025.

Chevalier, M., Davis, B. A. S., Heiri, O., Seppä, H., Chase, B. M., Gajewski, K., Lacourse, T., Telford, R. J., Finsinger, W., Guiot, J., Kühl, N., Maezumi, S. Y., Tipton, J. R., Carter, V. A., Brussel, T., Phelps, L. N., Dawson, A., Zanon, M., Vallé, F., Nolan, C., Mauri, A., de Vernal, A., Izumi, K., Holmström, L., Marsicek, J., Goring, S., Sommer, P. S., Chaput, M., and Kupriyanov, D.: Pollen-based climate reconstruction techniques for late Quaternary studies, Earth-Science Reviews, 210, 103384, https://doi.org/10.1016/j.earscirev.2020.103384, 2020.

Çolak, M. A., Öztaş, B., Özgencil, İ. K., Soyluer, M., Korkmaz, M., Ramírez-García, A., Metin, M., Yılmaz, G., Ertuğrul, S., Tavşanoğlu, Ü. N., Amorim, C. A., Özen, C., Apaydın Yağcı, M., Yağcı, A., Pacheco, J. P., Özkan,

K., Beklioğlu, M., Jeppesen, E., and Akyürek, Z.: Increased Water Abstraction and Climate Change Have Substantial Effect on Morphometry, Salinity, and Biotic Communities in Lakes: Examples from the Semi-Arid Burdur Basin (Turkey), Water, 14, 1241, https://doi.org/10.3390/w14081241, 2022.

Colleoni, F., Masina, S., Negri, A., and Marzocchi, A.: Plio–Pleistocene high–low latitude climate interplay: A Mediterranean point of view, Earth and Planetary Science Letters, 319–320, 35–44, https://doi.org/10.1016/j.epsl.2011.12.020, 2012.

Combourieu-Nebout, N., Bertini, A., Russo-Ermolli, E., Peyron, O., Klotz, S., Montade, V., Fauquette, S., Allen, J., Fusco, F., Goring, S., Huntley, B., Joannin, S., Lebreton, V., Magri, D., Martinetto, E., Orain, R., and Sadori, L.: Climate changes in the central Mediterranean and Italian vegetation dynamics since the Pliocene, Review of Palaeobotany and Palynology, 218, 127–147, https://doi.org/10.1016/j.revpalbo.2015.03.001, 2015.

Connor, S. E., Thomas, I., Kvavadze, E. V., Arabuli, G. J., Avakov, G. S., and Sagona, A.: A survey of modern pollen and vegetation along an altitudinal transect in southern Georgia, Caucasus region, Review of Palaeobotany and Palynology, 129, 229–250, https://doi.org/10.1016/j.revpalbo.2004.02.003, 2004.

Cravatte, J. and Suc, J.-P.: Climatic evolution of North-Western Mediterranean area during Pliocene and Early Pleistocene by pollen-analysis and forams of drill Autan 1. Chronostratigraphic correlations., Pollen et Spores, 23, 247–258, 1981.

Cugny, C., Mazier, F., and Galop, D.: Modern and fossil non-pollen palynomorphs from the Basque mountains (western Pyrenees, France): the use of coprophilous fungi to reconstruct pastoral activity, Veget Hist Archaeobot, 19, 391–408, https://doi.org/10.1007/s00334-010-0242-6, 2010.

Davies, C. P. and Fall, P. L.: Modern Pollen Precipitation from an Elevational Transect in Central Jordan and Its Relationship to Vegetation, Journal of Biogeography, 28, 1195–1210, 2001.

Davis, P. H., Cullen, J., and Coode, M. J. E. (Eds.): INTRODUCTION, in: Flora of Turkey and the East Aegean Islands, Volume 1, vol. 1, Edinburgh University Press, 1–26, 1965.

Davraz, A., Sener, E., and Sener, S.: Evaluation of climate and human effects on the hydrology and water quality of Burdur Lake, Turkey, Journal of African Earth Sciences, 158, 103569, https://doi.org/10.1016/j.jafrearsci.2019.103569, 2019.

De Schepper, S., Gibbard, P. L., Salzmann, U., and Ehlers, J.: A global synthesis of the marine and terrestrial evidence for glaciation during the Pliocene Epoch, Earth-Science Reviews, 135, 83–102, https://doi.org/10.1016/j.earscirev.2014.04.003, 2014.

Demirel, F. A. and Mayda, S.: A new Early Pleistocene mammalian fauna from Burdur Basin, SW Turkey, Rus.J.Theriol., 13, 55–63, https://doi.org/10.15298/rusjtheriol.13.2.01, 2014.

Dervişoğlu, A., Yağmur, N., Fıratlı, E., Musaoğlu, N., and Tanık, A.: Spatio-Temporal Assessment of the Shrinking Lake Burdur, Turkey, IJEGEO, 9, 169–176, https://doi.org/10.30897/ijegeo.1078781, 2022.

Diniz, F.: Etude palynologique du bassin pliocène de Rio Maior (Portugal), Paléobiologie continentale, 14, 259–267, 1984.

Djamali, M., de Beaulieu, J.-L., Campagne, P., Andrieu-Ponel, V., Ponel, P., Leroy, S. A. G., and Akhani, H.: Modern pollen rain–vegetation relationships along a forest–steppe transect in the Golestan National Park, NE Iran, Review of Palaeobotany and Palynology, 153, 272–281, https://doi.org/10.1016/j.revpalbo.2008.08.005, 2009.

Dugerdil, L., Joannin, S., Peyron, O., Jouffroy-Bapicot, I., Vannière, B., Boldgiv, B., Unkelbach, J., Behling, H., and Ménot, G.: Climate reconstructions based on GDGT and pollen surface datasets from Mongolia and Baikal area: calibrations and applicability to extremely cold–dry environments over the Late Holocene, Clim. Past, 17, 1199–1226, https://doi.org/10.5194/cp-17-1199-2021, 2021a.

Dugerdil, L., Ménot, G., Peyron, O., Jouffroy-Bapicot, I., Ansanay-Alex, S., Antheaume, I., Behling, H., Boldgiv, B., Develle, A.-L., Grossi, V., Magail, J., Makou, M., Robles, M., Unkelbach, J., Vannière, B., and Joannin, S.: Late Holocene Mongolian climate and environment reconstructions from brGDGTs, NPPs and pollen transfer

functions for Lake Ayrag: Paleoclimate implications for Arid Central Asia, Quaternary Science Reviews, 273, 107235, https://doi.org/10.1016/j.quascirev.2021.107235, 2021b.

El-Moslimany, A. P.: Ecological significance of common nonarboreal pollen: examples from drylands of the Middle East, Review of Palaeobotany and Palynology, 64, 343–350, https://doi.org/10.1016/0034-6667(90)90150-H, 1990.

Ezquerro, L., Muñoz, A., Liesa, C. L., Simón, J. L., and Luzón, A.: Late Neogene to Early Quaternary climate evolution in southwestern Europe from a continental perspective, Global and Planetary Change, 211, 103788, https://doi.org/10.1016/j.gloplacha.2022.103788, 2022.

Fauquette, S., Guiot, J., and Suc, J.-P.: A method for climatic reconstruction of the Mediterranean Pliocene using pollen data, Palaeogeography, Palaeoclimatology, Palaeoecology, 144, 183–201, https://doi.org/10.1016/S0031-0182(98)00083-2, 1998a.

Fauquette, S., Quézel, P., Guiot, J., and Suc, J.-P.: Signification bioclimatiquede taxons-guides du Pliocène méditerranéen, Geobios, 31, 151–169, https://doi.org/10.1016/S0016-6995(98)80035-1, 1998b.

Fauquette, S., Suc, J.-P., Guiot, J., Diniz, F., Feddi, N., Zheng, Z., Bessais, E., and Drivaliari, A.: Climate and biomes in the West Mediterranean area during the Pliocene, Palaeogeography, Palaeoclimatology, Palaeoecology, 152, 15–36, https://doi.org/10.1016/S0031-0182(99)00031-0, 1999.

Fauquette, S., Suc, J.-P., Bertini, A., Popescu, S.-M., Warny, S., Bachiri Taoufiq, N., Perez Villa, M.-J., Chikhi, H., Feddi, N., Subally, D., Clauzon, G., and Ferrier, J.: How much did climate force the Messinian salinity crisis? Quantified climatic conditions from pollen records in the Mediterranean region, Palaeogeography, Palaeoclimatology, Palaeoecology, 238, 281–301, https://doi.org/10.1016/j.palaeo.2006.03.029, 2006.

Fauquette, S., Suc, J. P., Jimenez-Moreno, G., Micheels, A., Jost, A., Favre, E., Bachiri, N., Bertini, T. A., Clet-Pellerin, M., Diniz, F., Farjanel, G., Feddi, N., and Zheng, Z.: Latitudinal climatic gradients in the Western European and Mediterranean regions from the Mid-Miocene (c. 15 Ma) to the Mid-Pliocene (c. 3.5 Ma) as quantified from pollen data, in: Deep-Time Perspectives on Climate Change: Marrying the Signal from Computer Models and Biological Proxies, edited by: Williams, M., Haywood, A. M., Gregory, F. J., and Schmidt, D. N., The Geological Society of London on behalf of The Micropalaeontological Society, 481–502, https://doi.org/10.1144/TMS002.22, 2007.

Feddi, N., Fauquette, S., and Suc, J.-P.: Histoire plio-pléistocène des écosystèmes végétaux de Méditerranée sud-occidentale : apport de l'analyse pollinique de deux sondages en mer d'Alboran, Geobios, 44, 57–69, https://doi.org/10.1016/j.geobios.2010.03.007, 2011.

Fedorov, A. V., Brierley, C. M., Lawrence, K. T., Liu, Z., Dekens, P. S., and Ravelo, A. C.: Patterns and mechanisms of early Pliocene warmth, Nature, 496, 43–49, https://doi.org/10.1038/nature12003, 2013.

Feng, R., Bhattacharya, T., Otto-Bliesner, B. L., Brady, E. C., Haywood, A. M., Tindall, J. C., Hunter, S. J., Abe-Ouchi, A., Chan, W.-L., Kageyama, M., Contoux, C., Guo, C., Li, X., Lohmann, G., Stepanek, C., Tan, N., Zhang, Q., Zhang, Z., Han, Z., Williams, C. J. R., Lunt, D. J., Dowsett, H. J., Chandan, D., and Peltier, W. R.: Past terrestrial hydroclimate sensitivity controlled by Earth system feedbacks, Nat Commun, 13, 1306, https://doi.org/10.1038/s41467-022-28814-7, 2022.

Ge, Y., Li, Y., Bunting, M. J., Li, B., Li, Z., and Wang, J.: Relation between modern pollen rain, vegetation and climate in northern China: Implications for quantitative vegetation reconstruction in a steppe environment, Science of The Total Environment, 586, 25–41, https://doi.org/10.1016/j.scitotenv.2017.02.027, 2017.

Gostyńska, J., Pankiewicz, R., Romanowska-Duda, Z., and Messyasz, B.: Overview of Allelopathic Potential of Lemna minor L. Obtained from a Shallow Eutrophic Lake, Molecules, 27, 3428, https://doi.org/10.3390/molecules27113428, 2022.

Gradstein, F. M. and Ogg, J. G.: Chapter 2 - The Chronostratigraphic Scale, in: Geologic Time Scale 2020, edited by: Gradstein, F. M., Ogg, J. G., Schmitz, M. D., and Ogg, G. M., Elsevier, 21–32, https://doi.org/10.1016/B978-0-12-824360-2.00002-4, 2020.

Grant, G. R., Naish, T. R., Dunbar, G. B., Stocchi, P., Kominz, M. A., Kamp, P. J. J., Tapia, C. A., McKay, R. M., Levy, R. H., and Patterson, M. O.: The amplitude and origin of sea-level variability during the Pliocene epoch, Nature, 574, 237–241, https://doi.org/10.1038/s41586-019-1619-z, 2019.

Grimm, E. C.: CONISS: a FORTRAN 77 program for stratigraphically constrained cluster analysis by the method of incremental sum of squares, Computers & Geosciences, 13, 13–35, https://doi.org/10.1016/0098-3004(87)90022-7, 1987.

Guiot, J.: Methodology of the last climatic cycle reconstruction in France from pollen data, Palaeogeography, Palaeoclimatology, Palaeoecology, 80, 49–69, https://doi.org/10.1016/0031-0182(90)90033-4, 1990.

Gürel, A. and Yıldız, A.: Diatom communities, lithofacies characteristics and paleoenvironmental interpretation of Pliocene diatomite deposits in the Ihlara–Selime plain (Aksaray, Central Anatolia, Turkey), Journal of Asian Earth Sciences, 30, 170–180, https://doi.org/10.1016/j.jseaes.2006.07.015, 2007.

Haywood, A. M., Dowsett, H. J., Valdes, P. J., Lunt, D. J., Francis, J. E., and Sellwood, B. W.: Introduction. Pliocene climate, processes and problems, Phil. Trans. R. Soc. A., 367, 3–17, https://doi.org/10.1098/rsta.2008.0205, 2009.

Haywood, A. M., Hill, D. J., Dolan, A. M., Otto-Bliesner, B. L., Bragg, F., Chan, W.-L., Chandler, M. A., Contoux, C., Dowsett, H. J., Jost, A., Kamae, Y., Lohmann, G., Lunt, D. J., Abe-Ouchi, A., Pickering, S. J., Ramstein, G., Rosenbloom, N. A., Salzmann, U., Sohl, L., Stepanek, C., Ueda, H., Yan, Q., and Zhang, Z.: Large-scale features of Pliocene climate: results from the Pliocene Model Intercomparison Project, Climate of the Past, 9, 191–209, https://doi.org/10.5194/cp-9-191-2013, 2013.

Haywood, A. M., Dowsett, H. J., and Dolan, A. M.: Integrating geological archives and climate models for the mid-Pliocene warm period, Nat Commun, 7, 10646, https://doi.org/10.1038/ncomms10646, 2016.

Haywood, A. M., Tindall, J. C., Dowsett, H. J., Dolan, A. M., Foley, K. M., Hunter, S. J., Hill, D. J., Chan, W.-L., Abe-Ouchi, A., Stepanek, C., Lohmann, G., Chandan, D., Peltier, W. R., Tan, N., Contoux, C., Ramstein, G., Li, X., Zhang, Z., Guo, C., Nisancioglu, K. H., Zhang, Q., Li, Q., Kamae, Y., Chandler, M. A., Sohl, L. E., Otto-Bliesner, B. L., Feng, R., Brady, E. C., von der Heydt, A. S., Baatsen, M. L. J., and Lunt, D. J.: The Pliocene Model Intercomparison Project Phase 2: large-scale climate features and climate sensitivity, Climate of the Past, 16, 2095–2123, https://doi.org/10.5194/cp-16-2095-2020, 2020.

Herbert, T. D., Ng, G., and Cleaveland Peterson, L.: Evolution of Mediterranean sea surface temperatures 3.5–1.5 Ma: Regional and hemispheric influences, Earth and Planetary Science Letters, 409, 307–318, https://doi.org/10.1016/j.epsl.2014.10.006, 2015.

Herzschuh, U., Tarasov, P., Wünnemann, B., and Hartmann, K.: Holocene vegetation and climate of the Alashan Plateau, NW China, reconstructed from pollen data, Palaeogeography, Palaeoclimatology, Palaeoecology, 211, 1–17, https://doi.org/10.1016/j.palaeo.2004.04.001, 2004.

Hijmans, R. J., Phillips, S., and Elith, J. L. and J.: dismo: Species Distribution Modeling, 2021.

Hilgen, F. J., Lourens, L. J., Van Dam, J. A., Beu, A. G., Boyes, A. F., Cooper, R. A., Krijgsman, W., Ogg, J. G., Piller, W. E., and Wilson, D. S.: Chapter 29 - The Neogene Period, in: The Geologic Time Scale, edited by: Gradstein, F. M., Ogg, J. G., Schmitz, M. D., and Ogg, G. M., Elsevier, Boston, 923–978, https://doi.org/10.1016/B978-0-444-59425-9.00029-9, 2012.

Horowitz, A.: Palynological evidence for the Quaternary rates of accumulation along the Dead Sea Rift, and structural implications, Tectonophysics, 164, 63–71, https://doi.org/10.1016/0040-1951(89)90234-5, 1989.

IPCC: Climate Change 2021: The Physical Science Basis. Contribution of Working Group I to the Sixth Assessment Report of the Intergovernmental Panel on Climate Change, Cambridge University Press., Cambridge, United Kingdom and New York, NY, USA, 2021.

IPCC: Climate Change 2023: Synthesis Report. Contribution of Working Groups I, II and III to the Sixth Assessment Report of the Intergovernmental Panel on Climate Change, Core Writing Team, H. Lee and J. Romero., Geneva, Switzerland, 2023.

Jankovská, V. and Komárek, J.: Indicative value ofPediastrum and other coccal green algae in palaeoecology, Folia Geobot, 35, 59–82, https://doi.org/10.1007/BF02803087, 2000.

Jiménez-Moreno, G. and Suc, J.-P.: Middle Miocene latitudinal climatic gradient in Western Europe: Evidence from pollen records, Palaeogeography, Palaeoclimatology, Palaeoecology, 253, 208–225, https://doi.org/10.1016/j.palaeo.2007.03.040, 2007.

Jiménez-Moreno, G., Popescu, S.-M., Ivanov, D., and Suc, J.-P.: Neogene flora, vegetation and climate dynamics in southeastern Europe and the northeastern Mediterranean, in: Deep-Time Perspectives on Climate Change: Marrying the Signal from Computer Models and Biological Proxies, vol. 2, edited by: Williams, M., Haywood, A. M., Gregory, F. J., and Schmidt, D. N., Geological Society of London, 0, https://doi.org/10.1144/TMS002.23, 2007.

Jiménez-Moreno, G., Fauquette, S., and Suc, J.-P.: Vegetation, climate and palaeoaltitude reconstructions of the Eastern Alps during the Miocene based on pollen records from Austria, Central Europe, Journal of Biogeography, 35, 1638–1649, https://doi.org/10.1111/j.1365-2699.2008.01911.x, 2008.

Jiménez-Moreno, G., Fauquette, S., and Suc, J.-P.: Miocene to Pliocene vegetation reconstruction and climate estimates in the Iberian Peninsula from pollen data, Review of Palaeobotany and Palynology, 162, 403–415, https://doi.org/10.1016/j.revpalbo.2009.08.001, 2010.

Jiménez-Moreno, G., Alçiçek, H., Alçiçek, M. C., Ostende, L. van den H., and Wesselingh, F. P.: Vegetation and climate changes during the late Pliocene and early Pleistocene in SW Anatolia, Turkey, Quaternary Research, 84, 448–456, https://doi.org/10.1016/j.yqres.2015.09.005, 2015.

Jiménez-Moreno, G., Anderson, R. S., Ramos-Román, M. J., Camuera, J., Mesa-Fernández, J. M., García-Alix, A., Jiménez-Espejo, F. J., Carrión, J. S., and López-Avilés, A.: The Holocene *Cedrus* pollen record from Sierra Nevada (S Spain), a proxy for climate change in N Africa, Quaternary Science Reviews, 242, 106468, https://doi.org/10.1016/j.quascirev.2020.106468, 2020.

Joly, C., Barillé, L., Barreau, M., Mancheron, A., and Visset, L.: Grain and annulus diameter as criteria for distinguishing pollen grains of cereals from wild grasses, Review of Palaeobotany and Palynology, 146, 221–233, https://doi.org/10.1016/j.revpalbo.2007.04.003, 2007.

Juggins, S.: Analysis of Quaternary Science Data. R package version 0.9-26., 2020.

Karaman, E.: Burdur dolayının genel stratigrafisi, Akdeniz Üniversitesi Isparta Mühendislik Fakültesi Dergisi, 2, 23–36, 1986.

Karas, C., Nürnberg, D., Bahr, A., Groeneveld, J., Herrle, J. O., Tiedemann, R., and deMenocal, P. B.: Pliocene oceanic seaways and global climate, Sci Rep, 7, 39842, https://doi.org/10.1038/srep39842, 2017.

Kaymakcı, N., Langereis, C., Özkaptan, M., Özacar, A. A., Gülyüz, E., Uzel, B., and Sözbilir, H.: Paleomagnetic evidence for upper plate response to a STEP fault, SW Anatolia, Earth and Planetary Science Letters, 498, 101–115, https://doi.org/10.1016/j.epsl.2018.06.022, 2018.

Kayseri-Özer, M. S., Karadenizli, L., Akgün, F., Oyal, N., Saraç, G., Şen, Ş., Tunoğlu, C., and Tuncer, A.: Palaeoclimatic and palaeoenvironmental interpretations of the Late Oligocene, Late Miocene–Early Pliocene in the Çankırı-Çorum Basin, Palaeogeography, Palaeoclimatology, Palaeoecology, 467, 16–36, https://doi.org/10.1016/j.palaeo.2016.05.022, 2017.

Komárek, J. and Marvan, P.: Morphological Differences in Natural Populations of the Genus *Botryococcus* (Chlorophyceae), Archiv für Protistenkunde, 141, 65–100, https://doi.org/10.1016/S0003-9365(11)80049-7, 1992.

Komárek, J. I. and Jankovská, V.: Review of the Green Algal Genus Pediastrum: Implication for Pollen-analytical Research, , 1–127, 2001.

Kottek, M., Grieser, J., Beck, C., Rudolf, B., and Rubel, F.: World Map of the Köppen-Geiger climate classification updated, metz, 15, 259–263, https://doi.org/10.1127/0941-2948/2006/0130, 2006.

Koutsodendris, A., Allstädt, F. J., Kern, O. A., Kousis, I., Schwarz, F., Vannacci, M., Woutersen, A., Appel, E., Berke, M. A., Fang, X., Friedrich, O., Hoorn, C., Salzmann, U., and Pross, J.: Late Pliocene vegetation turnover on the NE Tibetan Plateau (Central Asia) triggered by early Northern Hemisphere glaciation, Global and Planetary Change, 180, 117–125, https://doi.org/10.1016/j.gloplacha.2019.06.001, 2019.

Kristiansen, J. and Škaloud, P.: Chrysophyta, in: Handbook of the Protists, edited by: Archibald, J. M., Simpson, A. G. B., and Slamovits, C. H., Springer International Publishing, Cham, 331–366, https://doi.org/10.1007/978-3-319-28149-0_43, 2017.

Kuzucuoğlu, C.: The Physical Geography of Turkey: An Outline, in: Landscapes and Landforms of Turkey, edited by: Kuzucuoğlu, C., Çiner, A., and Kazancı, N., Springer International Publishing, Cham, 7–15, https://doi.org/10.1007/978-3-030-03515-0_2, 2019.

Lê, S., Josse, J., and Husson, F.: FactoMineR: An R Package for Multivariate Analysis, Journal of Statistical Software, 25, 1–18, https://doi.org/10.18637/jss.v025.i01, 2008.

Lee, C. M., Van Geel, B., and Gosling, W. D.: On the Use of Spores of Coprophilous Fungi Preserved in Sediments to Indicate Past Herbivore Presence, Quaternary, 5, 30, https://doi.org/10.3390/quat5030030, 2022.

Lefevre, C., Bellon, H., and Poisson, A.: Présence de leucitites dans le volcanisme pliocène de la région d'Isparta (Taurides occidentales, Turquie), C.-r. séances Acad. sci., Sér. 2 Méc.-phys. chim. sci. univers sci. terre, 297, 367–372, 1983.

Li, Y., Xu, Q., Yang, X., Chen, H., and Lu, X.: Pollen-vegetation relationship and pollen preservation on the Northeastern Qinghai-Tibetan Plateau, Grana, 44, 160–171, https://doi.org/10.1080/00173130500230608, 2005.

Li, Y., Bunting, M. J., Xu, Q., Jiang, S., Ding, W., and Hun, L.: Pollen–vegetation–climate relationships in some desert and desert-steppe communities in northern China, The Holocene, 21, 997–1010, https://doi.org/10.1177/0959683611400202, 2011.

Liaw, A. and Wiener, M.: Classification and Regression by randomForest, 2, 5, 2002.

Lisiecki, L. E. and Raymo, M. E.: A Pliocene-Pleistocene stack of 57 globally distributed benthic δ18O records, Paleoceanography, 20, https://doi.org/10.1029/2004PA001071, 2005.

Lytle, D. E. and Wahl, E. R.: Palaeoenvironmental reconstructions using the modern analogue technique: the effects of sample size and decision rules, The Holocene, 15, 554–566, https://doi.org/10.1191/0959683605hl830rp, 2005.

Ma, Y., Liu, K., Sang, Y., Wang, W., Sun, A., and Feng, Z. (Jordan): A Survey of Modern Pollen and Vegetation along a South-North Transect in Mongolia, Journal of Biogeography, 35, 1512–1532, 2008.

Magri, D. and Parra, I.: Late Quaternary western Mediterranean pollen records and African winds, Earth and Planetary Science Letters, 200, 401–408, https://doi.org/10.1016/S0012-821X(02)00619-2, 2002.

Masson-Delmotte, V., Schulz, M., Abe-Ouchi, A., Beer, J., Ganopolski, A., Gonzalez Rouco, J. F., Jansen, E., Lambeck, K., Luterbacher, J., Naish, T., Osborn, T., Otto-Bliesner, B., Quinn, T., Ramesh, R., Rojas, M., Shao, X., and Timmermann, A.: Information from paleoclimate archives, in: Climate Change 2013: The Physical Science Basis. Contribution of Working Group I to the Fifth Assessment Report of the Intergovernmental Panel on Climate Change, edited by: Stocker, T. F., Qin, D., Plattner, G.-K., Tignor, M. M. B., Allen, S. K., Boschung, J., Nauels, A., Xia, Y., Bex, V., and Midgley, P. M., Cambridge University Press, Cambridge, United Kingdom and New York, NY, USA, 383–464, https://doi.org/10.1017/CBO9781107415324.013, 2013.

Matthiessen, J. and Brenner, W.: Chlorococcalalgen und Dinoflagellaten-Zysten in rezenten Sedimenten des Greifswalder Boddens (südliche Ostsee), Senckenbergiana Maritima, 27, 33–48, 1996.

Medail, F. and Quézel, P.: Hot-Spots Analysis for Conservation of Plant Biodiversity in the Mediterranean Basin, Annals of the Missouri Botanical Garden, 84, 112–127, https://doi.org/10.2307/2399957, 1997.

Miller, K. G., Wright, J. D., Browning, J. V., Kulpecz, A., Kominz, M., Naish, T. R., Cramer, B. S., Rosenthal, Y., Peltier, W. R., and Sosdian, S.: High tide of the warm Pliocene: Implications of global sea level for Antarctic deglaciation, Geology, 40, 407–410, https://doi.org/10.1130/G32869.1, 2012.

Mudelsee, M. and Raymo, M. E.: Slow dynamics of the Northern Hemisphere glaciation, Paleoceanography, 20, https://doi.org/10.1029/2005PA001153, 2005.

Muller, S. D., Daoud-Bouattour, A., Fauquette, S., Bottollier-Curtet, M., Rifai, N., Robles, M., Saber, E.-R., El Madihi, M., Moukrim, S., and Rhazi, L.: Holocene history of peatland communities of central Rif (Northern Morocco), Geobios, S0016699522000018, https://doi.org/10.1016/j.geobios.2021.12.001, 2022.

Muñoz, A., Ojeda, J., and Sánchez-Valverde, B.: Sunspot-like and ENSO/NAO-like periodicities in lacustrinelaminated sediments of the Pliocene Villarroya Basin (La Rioja,Spain), Journal of Paleolimnology, 27, 453–463, 2002.

d'Oliveira, L., Dugerdil, L., Ménot, G., Evin, A., Muller, S. D., Ansanay-Alex, S., Azuara, J., Bonnet, C., Bremond, L., Shah, M., and Peyron, O.: Reconstructing 15 000 years of southern France temperatures from coupled pollen and molecular (branched glycerol dialkyl glycerol tetraether) markers (Canroute, Massif Central), Climate of the Past, 19, 2127–2156, https://doi.org/10.5194/cp-19-2127-2023, 2023.

Özkaptan, M., Kaymakci, N., Langereis, C. G., Gülyüz, E., Arda Özacar, A., Uzel, B., and Sözbilir, H.: Age and kinematics of the Burdur Basin: Inferences for the existence of the Fethiye Burdur Fault Zone in SW Anatolia (Turkey), Tectonophysics, 744, 256–274, https://doi.org/10.1016/j.tecto.2018.07.009, 2018a.

Özkaptan, M., Kaymakci, N., Langereis, C. G., Gülyüz, E., Arda Özacar, A., Uzel, B., and Sözbilir, H.: Age and kinematics of the Burdur Basin: Inferences for the existence of the Fethiye Burdur Fault Zone in SW Anatolia (Turkey), Tectonophysics, 744, 256–274, https://doi.org/10.1016/j.tecto.2018.07.009, 2018b.

Pagani, M., Liu, Z., LaRiviere, J., and Ravelo, A. C.: High Earth-system climate sensitivity determined from Pliocene carbon dioxide concentrations, Nature Geosci, 3, 27–30, https://doi.org/10.1038/ngeo724, 2010.

Panitz, S., Salzmann, U., Risebrobakken, B., De Schepper, S., and Pound, M. J.: Climate variability and long-term expansion of peatlands in Arctic Norway during the late Pliocene (ODP Site 642, Norwegian Sea), Climate of the Past, 12, 1043–1060, https://doi.org/10.5194/cp-12-1043-2016, 2016.

Peyron, O., Guiot, J., Cheddadi, R., Tarasov, P., Reille, M., de Beaulieu, J.-L., Bottema, S., and Andrieu, V.: Climatic Reconstruction in Europe for 18,000 YR B.P. from Pollen Data, Quat. res., 49, 183–196, https://doi.org/10.1006/qres.1997.1961, 1998.

Peyron, O., Bégeot, C., Brewer, S., Heiri, O., Magny, M., Millet, L., Ruffaldi, P., Van Campo, E., and Yu, G.: Late-Glacial climatic changes in Eastern France (Lake Lautrey) from pollen, lake-levels, and chironomids, Quat. res., 64, 197–211, https://doi.org/10.1016/j.yqres.2005.01.006, 2005.

Peyron, O., Goring, S., Dormoy, I., Kotthoff, U., Pross, J., de Beaulieu, J.-L., Drescher-Schneider, R., Vannière, B., and Magny, M.: Holocene seasonality changes in the central Mediterranean region reconstructed from the pollen sequences of Lake Accesa (Italy) and Tenaghi Philippon (Greece), The Holocene, 21, 131–146, https://doi.org/10.1177/0959683610384162, 2011.

Peyron, O., Magny, M., Goring, S., Joannin, S., de Beaulieu, J.-L., Brugiapaglia, E., Sadori, L., Garfi, G., Kouli, K., Ioakim, C., and Combourieu-Nebout, N.: Contrasting patterns of climatic changes during the Holocene across the Italian Peninsula reconstructed from pollen data, Clim. Past, 9, 1233–1252, https://doi.org/10.5194/cp-9-1233-2013, 2013.

Peyron, O., Combourieu-Nebout, N., Brayshaw, D., Goring, S., Andrieu-Ponel, V., Desprat, S., Fletcher, W., Gambin, B., Ioakim, C., Joannin, S., Kotthoff, U., Kouli, K., Montade, V., Pross, J., Sadori, L., and Magny, M.: Precipitation changes in the Mediterranean basin during the Holocene from terrestrial and marine pollen records: a model–data comparison, Clim. Past, 13, 249–265, https://doi.org/10.5194/cp-13-249-2017, 2017.

Pils, G.: Flowers of Turkey: A photo guide, Pemberley Natural History Books., Austria, 448 pp., 2006.

Plancq, J., Grossi, V., Pittet, B., Huguet, C., Rosell-Melé, A., and Mattioli, E.: Multi-proxy constraints on sapropel formation during the late Pliocene of central Mediterranean (southwest Sicily), Earth and Planetary Science Letters, 420, 30–44, https://doi.org/10.1016/j.epsl.2015.03.031, 2015.

Platevoet, B., Scaillet, S., Guillou, H., Blamart, D., Nomade, S., Massault, M., Poisson, A., Elitok, Ö., Özgür, N., Yagmurlu, F., and Yilmaz, K.: Pleistocene eruptive chronology of the Gölcük volcano, Isparta Angle, Turkey. Chronologie des épisodes volcaniques pléistocènes du volcan Gölcük, Angle d'Isparta, Turquie, Quaternaire. Revue de l'Association française pour l'étude du Quaternaire, 147–156, https://doi.org/10.4000/quaternaire.3092, 2008.

Popescu, S.-M.: Late Miocene and early Pliocene environments in the southwestern Black Sea region from high-resolution palynology of DSDP Site 380A (Leg 42B), Palaeogeography, Palaeoclimatology, Palaeoecology, 238, 64–77, https://doi.org/10.1016/j.palaeo.2006.03.018, 2006.

Popescu, S.-M., Biltekin, D., Winter, H., Suc, J.-P., Melinte-Dobrinescu, M. C., Klotz, S., Rabineau, M., Combourieu-Nebout, N., Clauzon, G., and Deaconu, F.: Pliocene and Lower Pleistocene vegetation and climate changes at the European scale: Long pollen records and climatostratigraphy, Quaternary International, 219, 152–167, https://doi.org/10.1016/j.quaint.2010.03.013, 2010.

Prasad, A. M., Iverson, L. R., and Liaw, A.: Newer Classification and Regression Tree Techniques: Bagging and Random Forests for Ecological Prediction, Ecosystems, 9, 181–199, https://doi.org/10.1007/s10021-005-0054-1, 2006.

Price, S. P. and Scott, B.: Pliocene Burdur basin, SW Turkey: tectonics, seismicity and sedimentation, Journal of the Geological Society, 148, 345–354, https://doi.org/10.1144/gsjgs.148.2.0345, 1991.

Quézel, P. and Médail, F.: Ecologie et biogéographie des foréts du bassin méditerranéen, Elsevier, 571 pp., 2003.

Ramezani, E.: Pollen–vegetation relationships in the central Caspian (Hyrcanian) forests of northern Iran, Review of Palaeobotany and Palynology, 12, 2013.

Raymo, M. E., Grant, B., Horowitz, M., and Rau, G. H.: Mid-Pliocene warmth: stronger greenhouse and stronger conveyor, Marine Micropaleontology, 27, 313–326, https://doi.org/10.1016/0377-8398(95)00048-8, 1996.

Reille, M.: Reille, Maurice, 1995. Pollen et spores d'Europe et d'Afrique du Nord, Supplément 1 . Éditions du Laboratoire de botanique historique et palynologie, Marseille, 327 p., 800 FF. / Reille, Maurice, 1998. Pollen et spores d'Europe et d'Afrique du Nord, Supplément 2. Éditions du Laboratoire de botanique historique et palynologie, Marseille, 530 p., 1600 FF., gpq, 52, 0–0, https://doi.org/10.7202/004885ar, 1998.

Robles, M., Peyron, O., Brugiapaglia, E., Ménot, G., Dugerdil, L., Ollivier, V., Ansanay-Alex, S., Develle, A.-L., Tozalakyan, P., Meliksetian, K., Sahakyan, K., Sahakyan, L., Perello, B., Badalyan, R., Colombié, C., and Joannin, S.: Impact of climate changes on vegetation and human societies during the Holocene in the South Caucasus (Vanevan, Armenia): A multiproxy approach including pollen, NPPs and brGDGTs, Quaternary Science Reviews, 277, 107297, https://doi.org/10.1016/j.quascirev.2021.107297, 2022.

Robles, M., Peyron, O., Ménot, G., Brugiapaglia, E., Wulf, S., Appelt, O., Blache, M., Vannière, B., Dugerdil, L., Paura, B., Ansanay-Alex, S., Cromartie, A., Charlet, L., Guédron, S., de Beaulieu, J.-L., and Joannin, S.: Climate changes during the Late Glacial in southern Europe: new insights based on pollen and brGDGTs of Lake Matese in Italy, Climate of the Past, 19, 493–515, https://doi.org/10.5194/cp-19-493-2023, 2023.

Salonen, J. S., Seppä, H., Luoto, M., Bjune, A. E., and Birks, H. J. B.: A North European pollen–climate calibration set: analysing the climatic responses of a biological proxy using novel regression tree methods, Quaternary Science Reviews, 45, 95–110, https://doi.org/10.1016/j.quascirev.2012.05.003, 2012.

Salonen, J. S., Korpela, M., Williams, J. W., and Luoto, M.: Machine-learning based reconstructions of primary and secondary climate variables from North American and European fossil pollen data, Sci Rep, 9, 15805, https://doi.org/10.1038/s41598-019-52293-4, 2019.

Salonen, J. S., Kuosmanen, N., Alsos, I. G., Heintzman, P. D., Rijal, D. P., Schenk, F., Bogren, F., Luoto, M., Philip, A., Piilo, S., Trasune, L., Väliranta, M., and Helmens, K. F.: Uncovering Holocene climate fluctuations

and ancient conifer populations: Insights from a high-resolution multi-proxy record from Northern Finland, Global and Planetary Change, 237, 104462, https://doi.org/10.1016/j.gloplacha.2024.104462, 2024.

Salzmann, U., Haywood, A. M., Lunt, D. J., Valdes, P. J., and Hill, D. J.: A new global biome reconstruction and data-model comparison for the Middle Pliocene, Global Ecology and Biogeography, 17, 432–447, https://doi.org/10.1111/j.1466-8238.2008.00381.x, 2008.

Salzmann, U., Dolan, A. M., Haywood, A. M., Chan, W.-L., Voss, J., Hill, D. J., Abe-Ouchi, A., Otto-Bliesner, B., Bragg, F. J., Chandler, M. A., Contoux, C., Dowsett, H. J., Jost, A., Kamae, Y., Lohmann, G., Lunt, D. J., Pickering, S. J., Pound, M. J., Ramstein, G., Rosenbloom, N. A., Sohl, L., Stepanek, C., Ueda, H., and Zhang, Z.: Challenges in quantifying Pliocene terrestrial warming revealed by data–model discord, Nature Clim Change, 3, 969–974, https://doi.org/10.1038/nclimate2008, 2013.

Saraç, G.: Vertebrate fossil localities of Turkey, Scientific Report No. 10609, Mineral Research and Exploration Directorate of Turkey (MTA)., Ankara, 208 pp., 2003.

Sassoon, D., Combourieu-Nebout, N., Peyron, O., Bertini, A., Toti, F., Lebreton, V., and Moncel, M.-H.: Pollen-based climatic reconstructions for the interglacial analogues of MIS 1 (MIS 19, 11, and 5) in the southwestern Mediterranean: insights from ODP Site 976, Climate of the Past, 21, 489–515, https://doi.org/10.5194/cp-21-489-2025, 2025.

Schwarz, F., Salzmann, U., Cheng, F., Ni, J., Nie, J., Patchett, M. R., Li, X., Li, L., Woodward, J., and Garzione, C.: High altitude Pliocene to Pleistocene vegetation and climate change of the Kunlun Pass Basin, NE Tibetan Plateau, Global and Planetary Change, 223, 104078, https://doi.org/10.1016/j.gloplacha.2023.104078, 2023.

Shatilova, I. I.: The palynological base of stratigraphical subdivision of late cainozoic deposits of the Western Transcaucasus, Review of Palaeobotany and Palynology, 48, 409–414, https://doi.org/10.1016/0034-6667(86)90077-1, 1986.

Sickenberg, O. and Tobien, H.: New Neogene and lower Quaternary vertebrate faunas in Turkey, Newsletters on Stratigraphy, 51–61, 1971.

Smol, J. P.: Chrysophycean microfossils in paleolimnological studies, Palaeogeography, Palaeoclimatology, Palaeoecology, 62, 287–297, https://doi.org/10.1016/0031-0182(88)90058-2, 1988.

Suc, J. P., Bertini, A., Combourieu-Nebout, N., Diniz, F., Leroy, S., Russo-Ermolli, E., Zheng, Z., Bessais, E., and Ferrier, J.: Structure of West Mediterranean vegetation and climate since 5.3 ma, Acta Zoologica Cracoviensia, 38, 1995.

Suc, J.-P.: Origin and evolution of the Mediterranean vegetation and climate in Europe, Nature, 307, 429–432, https://doi.org/10.1038/307429a0, 1984.

Suc, J.-P. and Cravatte, J.: Etude palynologique du Pliocène de Catalogne (Nord-Est de l'Espagne): apports à la connaissance de l'histoire climatique de la Méditerranée occidentale et implications chronostratigraphiques, Paléobiologie continentale, 13, 1–31, 1982.

Suc, J.-P., Popescu, S.-M., Fauquette, S., Bessedik, M., Jiménez-Moreno, G., Taoufiq, N. B., Zheng, Z., Medail, F., and Klotz, S.: Reconstruction of Mediterranean flora, vegetation and climate for the last 23 million years based on an extensive pollen dataset, Ecologia mediterranea, 44, 53, https://doi.org/10.3406/ecmed.2018.2044, 2018.

Tagliasacchi, E., Özer, M. S. K., and Altay, T.: Environmental, vegetational and climatic investigations during the Plio-Pleistocene in SW-Anatolia: A case study from the fluvio-lacustrine deposits in Uşak-Karahallı area, Palaeobio Palaeoenv, 104, 29–51, https://doi.org/10.1007/s12549-023-00590-2, 2024a.

Tagliasacchi, E., Özer, M. S. K., and Altay, T.: Environmental, vegetational and climatic investigations during the Plio-Pleistocene in SW-Anatolia: A case study from the fluvio-lacustrine deposits in Uşak-Karahallı area, Palaeobio Palaeoenv, 104, 29–51, https://doi.org/10.1007/s12549-023-00590-2, 2024b.

Tolotti, M., Thies, H., Cantonati, M., Hansen, C. M. E., and Thaler, B.: Flagellate algae (Chrysophyceae, Dinophyceae, Cryptophyceae) in 48 high mountain lakes of the Northern and Southern slope of the Eastern Alps:

biodiversity, taxa distribution and their driving variables, Hydrobiologia, 502, 331–348, https://doi.org/10.1023/B:HYDR.0000004291.03882.f7, 2003.

Tuncer, A., Karayigit, A. I., Oskay, R. G., Tunoğlu, C., Kayseri-Özer, M. S., Gümüş, B. A., Bulut, Y., and Akbulut, A.: A multi-proxy record of palaeoenvironmental and palaeoclimatic conditions during Plio-Pleistocene peat accumulation in the eastern flank of the Isparta Angle: A case study from the Şarkikaraağaç coalfield (Isparta, SW Central Anatolia), International Journal of Coal Geology, 265, 104149, https://doi.org/10.1016/j.coal.2022.104149, 2023.

Tweddle, J. C., Edwards, K. J., and Fieller, N. R. J.: Multivariate statistical and other approaches for the separation of cereal from wild Poaceae pollen using a large Holocene dataset, Veget Hist Archaeobot, 14, 15–30, https://doi.org/10.1007/s00334-005-0064-0, 2005.

Vaks, A., Woodhead, J., Bar-Matthews, M., Ayalon, A., Cliff, R. A., Zilberman, T., Matthews, A., and Frumkin, A.: Pliocene–Pleistocene climate of the northern margin of Saharan–Arabian Desert recorded in speleothems from the Negev Desert, Israel, Earth and Planetary Science Letters, 368, 88–100, https://doi.org/10.1016/j.epsl.2013.02.027, 2013.

Van Baak, C. G. C., Mandic, O., Lazar, I., Stoica, M., and Krijgsman, W.: The Slanicul de Buzau section, a unit stratotype for the Romanian stage of the Dacian Basin (Plio-Pleistocene, Eastern Paratethys), Palaeogeography, Palaeoclimatology, Palaeoecology, 440, 594–613, https://doi.org/10.1016/j.palaeo.2015.09.022, 2015.

Van Geel, B.: Non-Pollen Palynomorphs, in: Tracking Environmental Change Using Lake Sediments, vol. 3, edited by: Smol, J. P., Birks, H. J. B., Last, W. M., Bradley, R. S., and Alverson, K., Springer Netherlands, Dordrecht, 99–119, https://doi.org/10.1007/0-306-47668-1_6, 2002.

ten Veen, J. H., Boulton, S. J., and Alçiçek, M. C.: From palaeotectonics to neotectonics in the Neotethys realm: The importance of kinematic decoupling and inherited structural grain in SW Anatolia (Turkey), Tectonophysics, 473, 261–281, https://doi.org/10.1016/j.tecto.2008.09.030, 2009.

Wake, L. V. and Hillen, L. W.: Study of a “bloom” of the oil-rich alga Botryococcus braunii in the Darwin River Reservoir, Biotechnology and Bioengineering, 22, 1637–1656, https://doi.org/10.1002/bit.260220808, 1980.

Wang, P., Tian, J., and Lourens, L. J.: Obscuring of long eccentricity cyclicity in Pleistocene oceanic carbon isotope records, Earth and Planetary Science Letters, 290, 319–330, https://doi.org/10.1016/j.epsl.2009.12.028, 2010.

Wei, H. and Zhao, Y.: Surface pollen and its relationships with modern vegetation and climate in the Tianshan Mountains, northwestern China, Veget Hist Archaeobot, 25, 19–27, https://doi.org/10.1007/s00334-015-0530-2, 2016.

Wei, H., Ma, H., Zheng, Z., Pan, A., and Huang, K.: Modern pollen assemblages of surface samples and their relationships to vegetation and climate in the northeastern Qinghai-Tibetan Plateau, China, Review of Palaeobotany and Palynology, 163, 237–246, https://doi.org/10.1016/j.revpalbo.2010.10.011, 2011.

Westerhold, T., Marwan, N., Drury, A. J., Liebrand, D., Agnini, C., Anagnostou, E., Barnet, J. S. K., Bohaty, S. M., De Vleeschouwer, D., Florindo, F., Frederichs, T., Hodell, D. A., Holbourn, A. E., Kroon, D., Lauretano, V., Littler, K., Lourens, L. J., Lyle, M., Pälike, H., Röhl, U., Tian, J., Wilkens, R. H., Wilson, P. A., and Zachos, J. C.: An astronomically dated record of Earth’s climate and its predictability over the last 66 million years, Science, 369, 1383–1387, https://doi.org/10.1126/science.aba6853, 2020.

Willcox, G., Buxo, R., and Herveux, L.: Late Pleistocene and early Holocene climate and the beginnings of cultivation in northern Syria, The Holocene, 19, 151–158, https://doi.org/10.1177/0959683608098961, 2009.

Xiao, S., Li, S., Wang, X., Chen, L., and Su, T.: *Cedrus* distribution change: past, present, and future, Ecological Indicators, 142, 109159, https://doi.org/10.1016/j.ecolind.2022.109159, 2022.

Xu, Q., Li, Y., Tian, F., Cao, X., and Yang, X.: Pollen assemblages of tauber traps and surface soil samples in steppe areas of China and their relationships with vegetation and climate, Review of Palaeobotany and Palynology, 153, 86–101, https://doi.org/10.1016/j.revpalbo.2008.07.003, 2009.

Yavuz Işık, N., Saraç, G., Ünay, E., and de Bruijn, H.: Palynological Analysis of Neogene Mammal Sites of Turkey – Vegetational and Climatic Implications, Yerbilimleri, 32, 105–120, 2011.

Zhang, Y.-J., Duo, L., Pang, Y.-Z., Felde, V. A., Birks, H. H., and Birks, H. J. B.: Modern pollen assemblages and their relationships to vegetation and climate in the Lhasa Valley, Tibetan Plateau, China, Quaternary International, 467, 210–221, https://doi.org/10.1016/j.quaint.2018.01.040, 2018.

Zhao, Y. and Herzschuh, U.: Modern pollen representation of source vegetation in the Qaidam Basin and surrounding mountains, north-eastern Tibetan Plateau, Veget Hist Archaeobot, 18, 245–260, https://doi.org/10.1007/s00334-008-0201-7, 2009.

Zhao, Y., Yu, Z., and Chen, F.: Spatial and temporal patterns of Holocene vegetation and climate changes in arid and semi-arid China, Quaternary International, 194, 6–18, https://doi.org/10.1016/j.quaint.2007.12.002, 2009.

Zhao, Y., Li, Y., Zhang, Z., Fan, B., Zhu, Y., and Zhao, H.: Relationship between modern pollen assemblages and vegetation in the Bashang typical steppe region of North China, Ecological Indicators, 135, 108581, https://doi.org/10.1016/j.ecolind.2022.108581, 2022.

Zheng, Z., Huang, K., Xu, Q., Lu, H., Cheddadi, R., Luo, Y., Beaudouin, C., Luo, C., Zheng, Y., Li, C., Wei, J., and Du, C.: Comparison of climatic threshold of geographical distribution between dominant plants and surface pollen in China, Sci. China Ser. D-Earth Sci., 51, 1107–1120, https://doi.org/10.1007/s11430-008-0080-x, 2008.

Zheng, Z., Wei, J., Huang, K., Xu, Q., Tarasov, P., Luo, C., Beaudouin, C., Deng, Y., Zheng, Y., Luo, Y., Nakagawa, T., Li, C., Yang, S., Peng, H., and Cheddadi, R.: East Asian pollen database: modern pollen distribution and its quantitative relationship with vegetation and climate, Journal of Biogeography, 14, 2014.